Palaeogeography, Palaeoclimatology, Palaeoecology 649 (2024) 112332

Contents lists available at ScienceDirect

Palaeogeography, Palaeoclimatology, Palaeoecology

journal homepage: www.elsevier.com/locate/palaeo

The Messinian paleoenvironment in the Mediterranean (Monte dei Corvi, Ancona): A comparison with the modern oceanographic conditions

A.M. Mancini [a,b,*], S. Myers [a], R. Gennari [b], F. Lozar [b], A. Negri [a,*]

[a] Department of Life and Environmental Science, Università Politecnica delle Marche, 60122 Ancona, Italy
[b] Earth Sciences Department, Università degli Studi di Torino, 10125 Torino, Italy

ARTICLE INFO

Editor: M Elliot

Keywords:
Calcareous nannofossil
Foraminifer
Anoxia
Sapropel
Climate change

ABSTRACT

The Messinian was characterized by peculiar biogeochemical dynamics and climate in the Mediterranean region, testified by widespread deoxygenation events (sapropel) and evaporite deposition. To constrain the Mediterranean response to past perturbation it is crucial to understand the current environmental crisis related to climate change. In this regard, benthic and planktic calcareous fossils provide valuable insights into surface and bottom water conditions during deoxygenation events.

Here we studied in high resolution 4 sapropel-bearing cycles of the Monte dei Corvi (Ancona, Italy), which recorded the behavior of the Adriatic Deep-Water formation, a major controlling factor for the oxygenation in the modern Eastern Mediterranean. Our analysis unveils fluctuations in planktic and benthic assemblages driven by variations in insolation parameters. Sapropel interbeds deposited during insolation maxima exhibit warm-oligotrophic and Deep Chlorophyll Maximum taxa, suggesting warming and freshening of surface water, leading to weakened Adriatic Deep-Water formation and reduced oxygen delivery to the bottom. Marly limestone/marlstone interbeds exhibit the dominance of cold-eutrophic taxa and an abundance of fecal pellets with monospecific/oligospecific calcareous nannofossils taxa (*Umbilicosphaera jafari* and *Reticulofenestra perplexa*), suggesting moderately high salinity and sustained productivity during phases of strong mixing.

Comparisons between Messinian and the present-day setting reveal significant differences in the abundance and distribution of calcareous planktic assemblage, mostly due to heightened productivity during the Messinian, a response to restricted conditions that increased the basin's susceptibility to nutrient-delivering runoff. This circumstance played a significant role in the widespread deoxygenation and accumulation of organic carbon during the Messinian.

The uncertain trajectory of primary production in the Mediterranean complicates precise predictions of the future oxygen balance. Insights from the Messinian underscore the crucial role of primary productivity in shaping bottom oxygen conditions, emphasizing the necessity for ongoing investigations.

1. Introduction

Over the last 15 Ma, the Mediterranean has witnessed cyclical and widespread deoxygenation events, represented by organic-rich sediment layers known as sapropels (Taylforth et al., 2014; Athanasiou et al., 2021). The sapropels are believed to have formed in response to climatic and oceanographic changes that collectively weakened the thermohaline circulation and potentially enhanced primary productivity (De Lange et al., 2008; Rohling et al., 2015; Blanchet et al., 2021; Mancini et al., 2024b). Understanding the Mediterranean's oxygen balance in response to climate and environmental alteration is crucial for developing effective mitigation or adaptation strategies, as oxygen starvation can profoundly impact marine ecosystems and services (Diaz and Rosenberg, 2008; Mancini et al., 2024b). In this context, unraveling the paleoceanographic regime and associated thermohaline circulation behavior during a "warmer than present" interval stands as a pivotal keystone in comprehending climate change effects. The extreme Messinian pre-evaporitic setting, characterized by warmer sea surface temperatures (SST) (Tzanova et al., 2015; Mayser et al., 2017; Vasiliev et al., 2019; Kontakiotis et al., 2022; Butiseacă et al., 2022) and heightened Mediterranean restriction compared to today, represents a candidate for such investigation (Mancini et al., 2024a). Indeed, the Messinian was characterized by a progressive restriction that proceeded by step (Flecker et al., 2015; Corbí et al., 2020). The pre-evaporitic phase ends

* Corresponding authors at: Department of Life and Environmental Science, Università Politecnica delle Marche, 60122 Ancona, Italy.

https://doi.org/10.1016/j.palaeo.2024.112332
Received 12 March 2024; Received in revised form 10 June 2024; Accepted 10 June 2024
Available online 11 June 2024

with the climax phase of restriction and the establishment of the Messinian Salinity Crisis (Corbí et al., 2020), one of the most recent extreme events affecting the Mediterranean, characterized by conspicuous deposition of evaporites (Roveri et al., 2014).

In recent decades, the Mediterranean has undergone profound environmental disturbances, directly or indirectly attributable to human activities. The effects of global climate change are more marked in the Mediterranean area, making it a climate change hotspot (Giorgi, 2006; Lionello and Scarascia, 2018). The Eastern Mediterranean is ranked as an oligotrophic region, with phosphorus acting as a limiting nutrient for phytoplankton growth (Krom et al., 2004). Consequently, any abrupt increase in phosphorus entering the photic zone can trigger heightened primary productivity, potentially leading to eutrophication and increasing oxygen consumption. The Mediterranean is marked by several hypoxic sites (Viaroli et al., 2015), commonly referred to as "dead zones," due to the adverse impact of oxygen limitation on marine organisms. In recent decades, the Mediterranean has experienced warming and drying trends, which are expected to intensify in the near future (Somot et al., 2006; Sakalli, 2017; MedECC, 2020). Like eutrophication, the warming trend threatens the oxygen balance but with different pathways: it reduces oxygen solubility, impacts thermohaline circulation and mixed layer depth, while concurrently increasing the metabolism and thus the oxygen consumption by marine organisms through remineralization of organic matter (Breitburg et al., 2018; Limburg et al., 2020; Mancini et al., 2024b). The observed decline in thermohaline circulation strength and the expansion of dead zones in recent decades (Diaz and Rosenberg, 2008; Altieri and Gedan, 2015; Breitburg et al., 2018; Limburg et al., 2020) can be early warning signals for more extensive deoxygenation events, propelled by the accelerating pace of climate warming (Mancini et al., 2024b).

In this paper, we present the result of an ultra-high-resolution study of the micropaleontological content (calcareous nannofossil and foraminifer) in the Messinian Monte dei Corvi sedimentary succession, spanning $\approx$ 100 Ka and characterized by cyclical oceanographic changes, represented by alternance of sapropel and marly-limestone layers. This lithological alternance represents the variation in the Adriatic Deep Water (ADW) formation system (Mancini et al., 2024a); hence, offering valuable insights into the fluctuations of surface and bottom water conditions, which are pivotal factors in the process of deoxygenation. The ADW formation system, identified as a significant oxygen source in the Eastern Mediterranean deep setting (Rohling et al., 2015; Schroeder et al., 2023), underscores the relevance of investigating these variations. Additionally, we compiled existing Messinian micropaleontological data from Mediterranean localities to evidence the main oceanographic differences compared to the modern setting, the latter provided by Azibeiro et al. (2023). This comparison allows speculations on the future oceanographic conditions associated with warming.

2. Messinian and modern Mediterranean oceanographic setting

The circulation of the Mediterranean water masses relies on precipitation and evaporation balance, which determine an anti-estuarine circulation, with low-density superficial Atlantic water inflow and the denser salty Mediterranean bottom water outflow at Gibraltar. From a biogeochemical perspective, the Mediterranean is considered a heterotrophic basin, where oxygen is consumed more than its production (Duarte et al., 2013; Powley et al., 2017). The oxygenation of the Mediterranean abysses relies on buoyancy loss and sinking of surface waters.

Schematically, surficial and relatively cold low salinity waters enter the Mediterranean from the Atlantic and, flowing eastward, they progressively gain salinity and temperature because of strong net evaporation, setting the stage for a complex thermohaline circulation within the basin, that orchestrates the distribution of temperature, salinity, and crucially, oxygen content (Schroeder et al., 2023). In this framework, the Adriatic region emerges as a pivotal player during the winter months when deep water formation occurs in response to cold winds, giving rise to the Northern Adriatic dense Water (NadDW), which sinks near the Middle Adriatic pit forming the ADW (Artegiani et al., 1997; Rohling et al., 2015; Schroeder et al., 2023). This system was recognized as the principal deep-water formation site in the Eastern Mediterranean (Schroeder et al., 2023). Similarly, in winter, the Levantine Sea experiences a cooling effect, causing surface water to increase in density. This phenomenon facilitates the creation of the Levantine Intermediate Water (LIW), typically found between depths of 150 and 600 m. The area near Rhodes is important for the LIW formation, although the formation area can be extended to the whole Levantine basin (Nittis and Lascaratos, 1998; Schroeder et al., 2012). Part of the LIW moves westward and accounts for a portion of the Mediterranean outflow water (MOW), but part flows northward along the eastern Adriatic and finally mixes with the cool superficial water, contributing to the ADW formation system (Tzanova et al., 2015). In the Western Mediterranean, the deep water (WMDW) is formed in the Gulf of Lyon area, where cold winds during winter favor deep convection. Furthermore, the Bernoulli aspiration acting at the Gibraltar Strait, further facilitates the WMDW formation (Rohling et al., 2015).

One of the features causing the different oceanographic regime between the Messinian and the modern setting is the configuration of the Gibraltar Strait, which was shallower/narrower in response to the tectonic activity (Roveri et al., 2014; Flecker et al., 2015; Krijgsman et al., 2018). A restricted Gibraltar limited the water exchange with the Atlantic and not only extended the residence time of bottom water (Kouwenhoven et al., 2006; Bulian et al., 2022), but also likely resulted in higher salinities in the deeper layers (Meijer, 2006). This is because a shallower strait would reduce the Bernoulli aspiration depth, causing a gradual increase in the saltiness and density of deep waters. This heightened density contrast between the Atlantic inflow and the Mediterranean intermediate/deep-water masses favored the stratification of the water column, as indicated by box models (Meijer, 2006). Consequently, this scenario would lead to less efficient deep water circulation and an ensuing prolonged bottom water residence time (Kouwenhoven et al., 1999; Sierro et al., 2003; Bulian et al., 2022), favoring deoxygenation. However, some features are thought to be mostly unchanged, like the circulation patterns of the Eastern Mediterranean and Adriatic areas (Kouwenhoven and Van der Zwaan, 2006). Indeed, in-depth examinations of micropaleontological data indicate the presence of an intermediate water mass resembling the contemporary LIW, flowing at depths between 200 and 600 m during the Messinian (Kouwenhoven and Van der Zwaan, 2006).

3. Material and method

3.1. Geological setting and sampling

The studied section was previously referred to as "Monte Dei Corvi Beach" (Hüsing et al., 2009) and is located south of Ancona along the shoreline between Monte dei Corvi and Mezzavalle beaches (43° 34′N, 13° 34′E; Fig. 1 and Fig. 2). The studied interval is characterized by hemipelagic sedimentation and belongs to the pre-evaporitic phase of the Messinian salinity crisis (Roveri et al., 2005), termed "Euxinic Shale Interval" in the outer Apennine foredeep (Roveri et al., 2005; Hüsing et al., 2009). The upper part of the section is covered by vegetation and landslides, hiding the contact between the pre-evaporitic to evaporitic sediment pertaining to the "Gessoso-Solfifera" Formation (Roveri et al., 2005). As in the rest of the Mediterranean (Krijgsman et al., 2004), the studied interval is characterized by sedimentary cycles deposited under precessional control. The cycles are made up of sapropel, packstone and marly limestone/marlstone layers (Mancini et al., 2024a). The sapropels are characterized by variable total organic content, from 1.5% to 3.0% (Mancini et al., 2024a), therefore in some cases they do not fall under the classic sapropel definition proposed by Kidd et al. (1978), but agree with the less restrictive definition proposed by Hilgen (1991). The

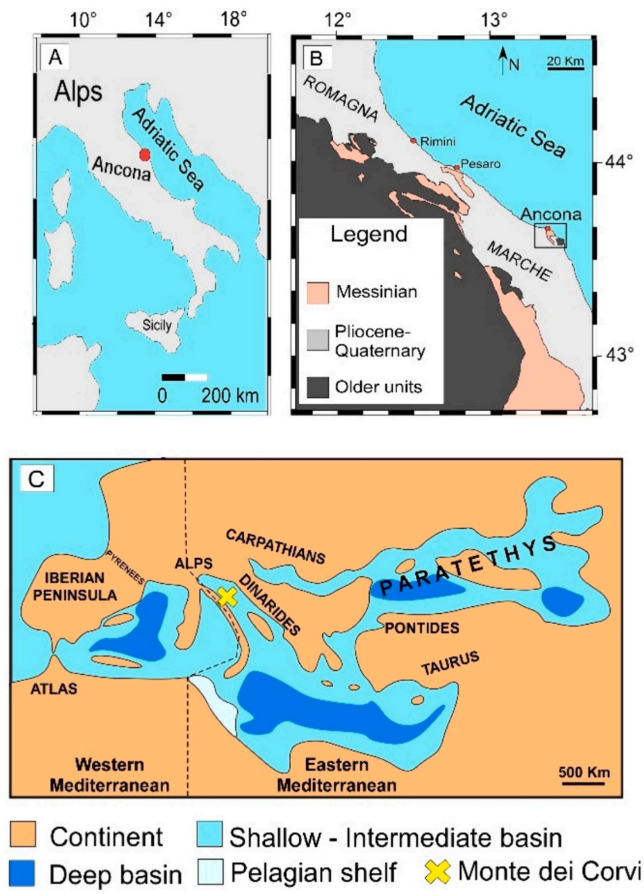

Fig. 1. Geological and paleogeographic map of the studied area.
A and B: Location and simplified geological map of the studied area. The studied section is indicated by the black square in B.
C: Paleogeographic reconstruction of the Mediterranean during the early Messinian with the location of the studied area. Modified after Popov et al. (2004).

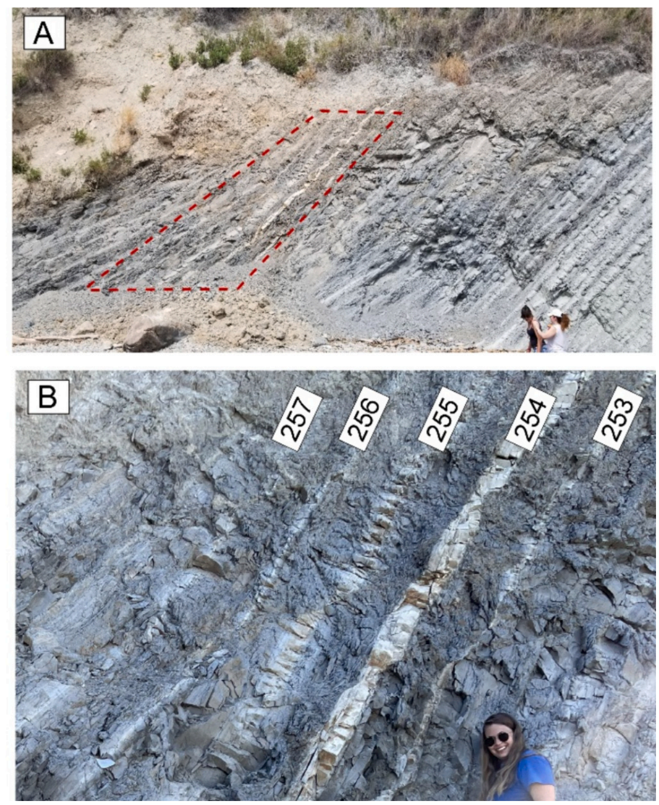

Fig. 2. Pictures detailing the cycles of the Monte dei Corvi section.
A: Outcrop view with the analyzed interval (dashed red polygon).
B: Close-up of the analyzed interval with cycles numbered according to Hüsing et al. (2009).

sapropels are dark, organic-rich and laminated marlstone deposited during insolation maxima (precession minima) (Fig. 3). The lamination is made up of black-brown and white-grey laminae composed of silt-sized terrigenous and pyrite grains and by peloids and fecal pellets, respectively (Fig. 3). Packstone layers are 1–4 cm thick and are composed of sand-sized foraminifer, glauconite and burrowing (Fig. 3) and are interpreted as the results of vigorous bottom current related to thermohaline circulation (i.e ADW formation) during insolation minima (precession maxima) (Mancini et al., 2024a). Mancini et al. (2024a) indicate that the sedimentary record is cyclically erased since the base of the packstone layers shows erosional contact with the underlying sapropels. The marly limestone/marlstone interbeds are usually laminated, showing alternation of grey-white and brown-dark lamina (Fig. 3). The grey-white laminae are made up of fecal pellets (average size ~200 μm) primarily composed of oligospecific or monospecific calcareous nannofossil assemblage (Fig. 3).

We collected 99 samples for the calcareous nannofossils analysis and 66 for the foraminifer analysis (Fig. 4). A subset of 40 samples were previously analyzed for mineralogical, sedimentological, petrographic and geochemical analysis by Mancini et al. (2024a).

3.2. Foraminifer analysis

A variable quantity (100–250 g) of samples were dry weighed, freeze-dried, soaked with diluted H_2O_2, and washed with tap water over a 63 μm mesh size sieve. The residues were dried in an oven at 40 °C overnight and dry-sieved over a 125 μm sieve. Samples collected in the limestone layers and slightly above or below (depths 64 and 211 cm) required more time to be soaked and washed due to strong cementation. Samples at depths 11.5, 70.5, and 115 cm were not completely disaggregated, casting doubt on the reliability of their results. For each sample, planktic and benthic foraminiferal counts were carried out separately on subsamples of at least 150–300 individuals of the >125 μm size fraction. The specimens were hand-picked and, where possible, identified to the species level as preservation allowed, and counted. Entire samples were used when the total number of foraminifer was very small. The raw counts were transformed into absolute abundance (individual per gram of dry sediment) and relative abundance (%). Sinistrally and dextrally coiled *Neogloboquadrina acostaensis* were counted as separate species and all *Orbulina* taxa (*O. universa* and *O. suturalis*) were lumped together. Based on ecological preferences according to Murray (2006), *Ammonia* spp., *Elphidium, Neoconorbina terquemi, Lobatula lobatula, Porosononion granosum, Fissurina marginata,* and *Hanzawaia boueana* were lumped together as "inner shelf" species.

Following Sierro et al. (1999, 2003), to recognize the planktic foraminifer assemblage response to the cyclical oceanographic changes of this setting, we calculated the ratio between planktic species that indicate "warm, oligotrophic" (W—O) water (*Globigerinoides elongatus, Globigerinoides obliquus, Globigerinoides ruber, Globigerinoides tenellus, Globigerinoides extremus, Orbulina gr.)* and "cold, eutrophic" (C-E) water *(Globigerina bulloides, Globigerinita glutinata, Neogloboquadrina acostaensis* (dextral), *Neogloboquadrina acostaensis* (sinistral), *Neogloboquadrina incompta, Neogloboquadrina pachyderma, Turborotalita multiloba, Turborotalita quinqueloba*).

The preservation of planktic and benthic foraminifer was moderate to good in the sapropel samples, while it was poor to moderate in the marly limestone/marlstone samples. No significant differences were observed in the preservation of planktic and benthic foraminifer within

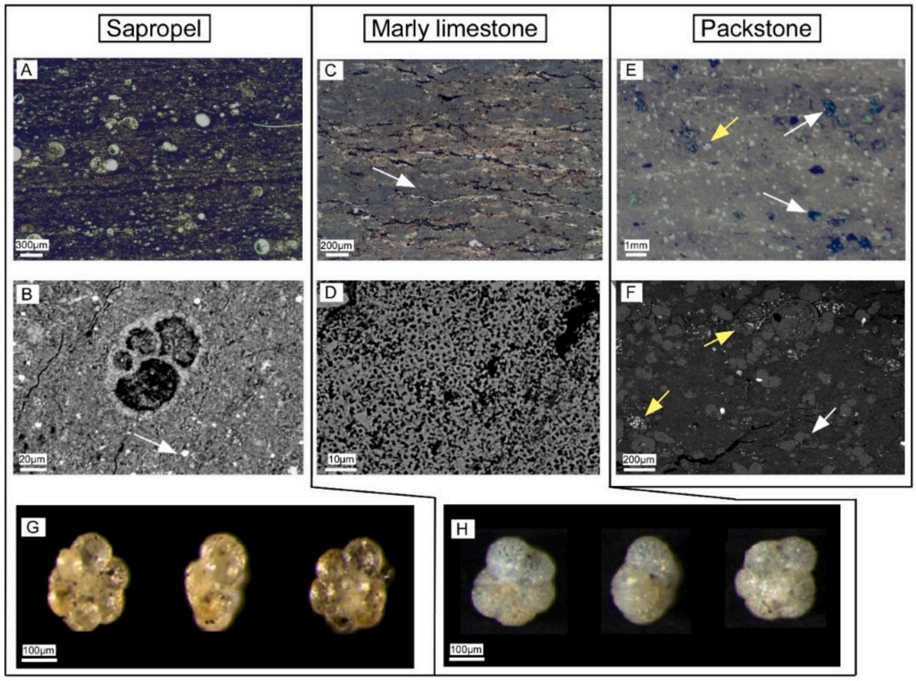

Fig. 3. Thin section and hand-picked foraminifer photomicrographs of the different lithofacies at optical microscope (A, C, E, G and H) and SEM (B; D and F). A) Sapropel of cycle 254 showing distinct lamination and planktic foraminifer. B) Enlargement of A showing well-preserved planktic foraminifer and diffused pyrite (white arrow). C) Marly limestone of cycle 253 showing lamination made up of grey laminae (white arrow) composed of fecal pellets and brown laminae composed of terrigenous materials. D) Magnification of a fecal pellet that composes the grey laminae showing monospecific assemblage of *U. Jafari.* E) Packstone of cycle 253 showing sand-sized glauconite minerals (white arrows) and foraminifer (yellow arrow). F) Magnification of E showing foraminifer (white arrows) and burrows filled with pyrite (yellow arrow). G and H) The taxon *T. multiloba* recorded in the marly limestone and sapropel samples.

the same sample. The P/B ratio was calculated using the formula P/(P + B)*100, where P and B represent the absolute abundance of planktic and benthic foraminifer, respectively. We also calculated the enhanced Benthic Foraminifer Oxygen Index (EBFOI), using the equation of Kranner et al. (2022) that can be converted to provide dissolved oxygen values (mL/L) of the bottom water. Since in literature the succession is interpreted as an outer shelf setting (Iaccarino et al., 2008) we excluded from this calculation all the inner shelf taxa (see 5.1 paragraph). The diversity index (Shannon index) was calculated for each sample, using the PAST (PAleontological STatistics) software package (Hammer and Harper, 2001). This index shows how much the assemblage is diverse and is used here as an indication of oligotrophy and stability of the ecosystem, because such environmental conditions are usually characterized by more diverse planktic foraminifer and calcareous nannofossil assemblage (Winter, 1994; Baumann et al., 2005; Schiebel and Hemleben, 2017).

3.3. *Calcareous nannofossil analysis*

Standard smear slides were prepared for each sample and observed at 1250 X by light microscope. For each slide, at least 400 specimens (excluding the reworked) were counted and taxonomically identified, along with a qualitative assessment of the preservation performed additionally with SEM inspection of sediment chip and thin sections. The taxa *Reticulofenestra pseudoumbilicus* < 7 µm and > 7 µm, *Calcidiscus leptoporus* < 7 µm and > 7 µm, *Pontosphaera multipora*, *P. japonica*, *Discoaster variabilis*, *D. brouweri*, *D. pentaradiatus*, *Sphenolithus abies* and *S. moriformis* are included in the informal groups of *R. pseudoumbilicus* gr., *C. leptoporus* gr., *Pontosphaera* gr., *Discoaster* gr. and *Sphenolithus* gr., respectively.

The taxa *Sphenolithus* spp. and *Discoaster* spp. were grouped to highlight differences in the SST, since these taxa are widely reported as proliferating in warm and possibly stratified environments (Perch-Nielsen, 1985; Gibbs et al., 2004; Flores et al., 2005; Violanti et al., 2013; Mancini et al., 2020). The Shannon index was calculated for each sample, as it was for the foraminifer.

3.4. *Statistical analysis*

Principal Component Analysis (PCA) were conducted for planktic foraminifer and calcareous nannofossils using prcomp()“ function in the “stats” R package and plotted using ggplot(). The PCA was obtained using only the species and groups that show maximum abundances >3%. The PCA analyses show the taxa with similar paleoecological requirements and how they are distributed over a range of environmental components that are responsible for the assemblage fluctuations. Based on the PCA results, the taxa which aligns following the PC axis are grouped. The analysis excluded benthic foraminifer due to limitations in sample size and the relatively lower number of taxa recorded compared to other fossil groups.

4. Results

4.1. *Planktic foraminifer*

Planktic foraminifera are good to moderately preserved throughout the studied section, showing two distinct peaks in abundance corresponding to the marly limestone layers of cycle 255 and the top of sapropel 256 (Fig. 5). A total of 29 taxa were recovered with *T. quinqueloba* being the dominant species, followed by *O. universa*, *Globoturborotalita rubescens*, *T. multiloba*, and *N. acostaensis* (dextral). Other subordinated taxa are *Globigerinoides* spp., *Globigerina falconensis, G. bulloides, Globigerinita glutinata* and *Globigerinita* spp. In detail, *T. quinqueloba and T. multiloba* show clear peaks spanning from each limestone layer to the base of the following sapropels; *T. multiloba* peaks gradually increase upward throughout the study section (Fig. 5).

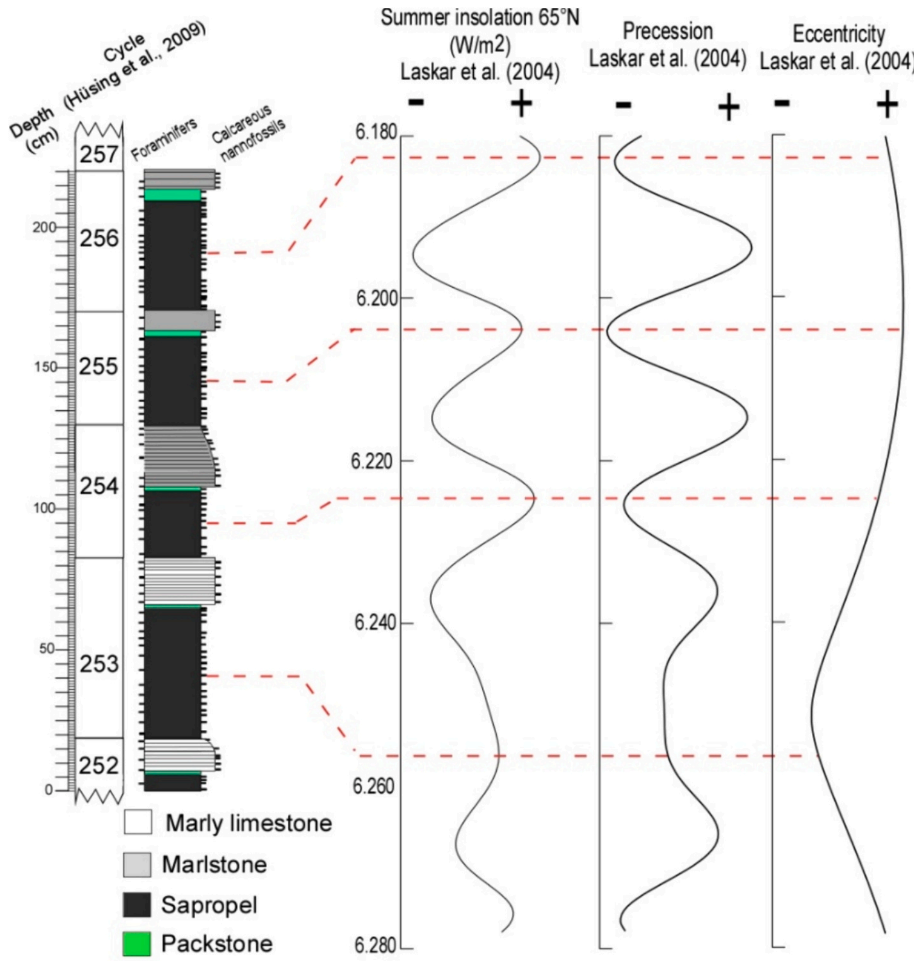

Fig. 4. Stratigraphic column of the analyzed interval in relation to summer insolation, precession and eccentricity at 65°N of Laskar et al. (2004).

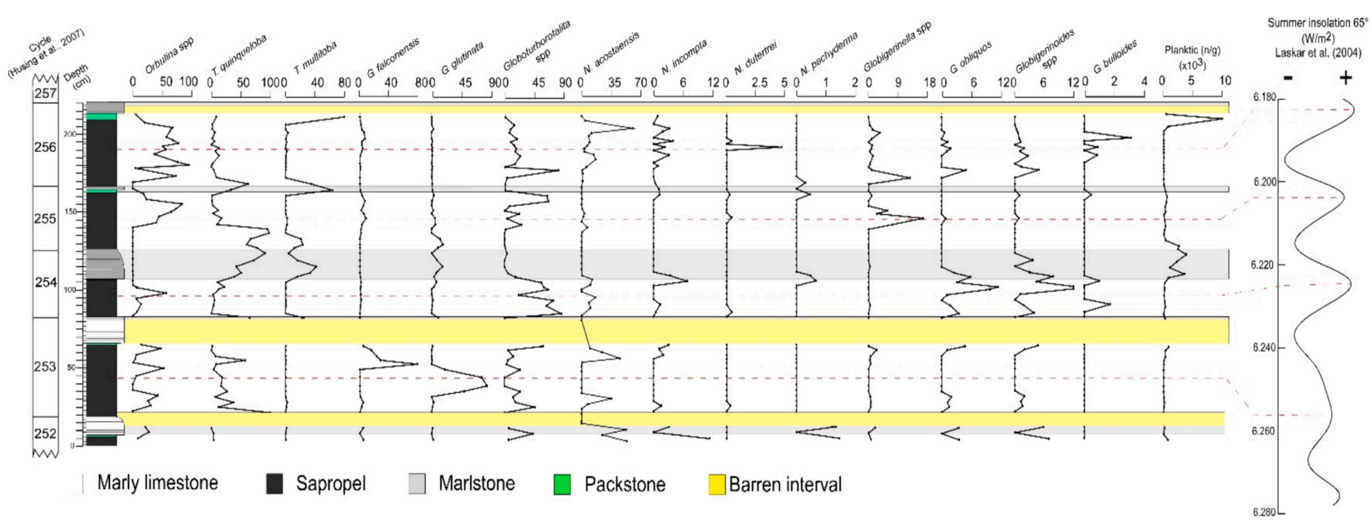

Fig. 5. Planktic foraminifer relative and absolute abundance in relation to the summer insolation at 65°N (Laskar et al., 2004). The horizontal dotted red line indicates the sapropel mid-point. (For interpretation of the references to colour in this figure legend, the reader is referred to the web version of this article.)

Orbulina spp. and *Globoturborotalita* spp. have similar abundance trends and, although fluctuating, show generally high abundances in the sapropels and are nearly absent in the limestone layers (apart from cycle 253 limestone) (Fig. 5). Neogloboquadrinids also prevalently occur in sapropels (Fig. 5).

4.2. *Benthic foraminifer*

Benthic foraminifer are rare throughout the section except for five peaks occurring in, or close to the limestone layers (Fig. 6). A total of 19 samples are barren or show very bad preservation/abundance that

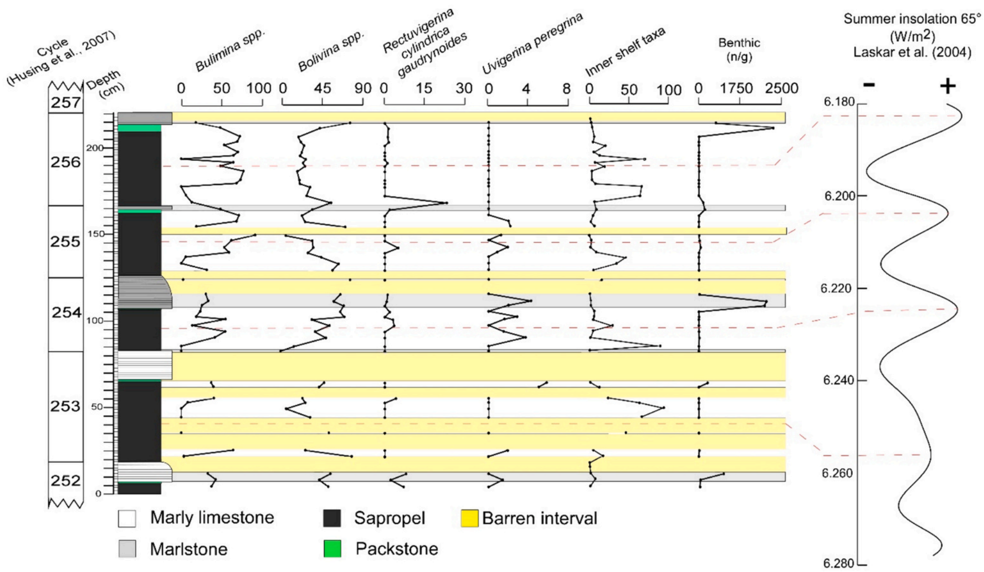

Fig. 6. Benthic foraminifer relative and absolute abundance in relation to the summer insolation at 65°N (Laskar et al., 2004). The horizontal dotted red line indicates the sapropel mid-point, while the yellow rectangles indicate samples barren of benthic foraminifer. (For interpretation of the references to colour in this figure legend, the reader is referred to the web version of this article.)

hinders counting; the remaining samples show good to moderately preserved benthic foraminifer throughout the studied section. A total of 29 taxa were recovered with *Bolivina* spp. being the dominant genus (mainly *B. dilatata*, *B. spathulata*, and *B. plicatella*) followed by *Bulimina* spp. (mainly *B. aculeata*) and *Lobatula lobatula* (Fig. 6). The remaining taxa are subordinate. Importantly, inner shelf taxa were found throughout the section and showed a trend of increased relative abundance within the sapropels (especially in the basal portion) while they are nearly absent within the limestone (Fig. 6). *Bolivina* spp. is relatively more abundant in cycles 253 and 254 and is progressively replaced by *Bulimina* spp., which increase in cycles 255 and 256. *Uvigerina* sp. shows low percentages throughout the record with peaks occurring within the sapropels, except in cycle 256 (Fig. 6).

4.3. Calcareous nannofossil

Calcareous nannofossil are usually moderate to well preserved throughout the studied section. The most abundant taxa are *R. minuta* and *U. jafari*, which tend to dominate the assemblage. Specifically, *U. jafari* shows prominent peaks in abundance (up to 98%) in the marly limestone/marlstone of cycles 253 and 254 (Fig. 7). In the marlstone of cycles 255, 256 and 257 *U. jafari* is progressively replaced by *R. perplexa*, which shows high abundances up to 57%. *Reticulofenestra haqii* and *S. abies* show moderate abundances (on average between 10% - 20%) in the sapropels, whereas their abundances drop in the marly limestone/marlstone layers (Fig. 7). The *Discoaster* group and *U. rotula* are present in the sapropels in low abundance, generally not exceeding 7% and 3% respectively, while their abundance in the marly limestone/marlstone layers does not exceed 1.5% (Fig. 7). The taxa *Helicosphaera carteri* and *Pontosphaera* gr. are scarce except for prominent peaks preceding or in the packstone layers, these peaks are followed by peaks of *C. leptoporus* gr. at the base of each marly limestone/marlstone layer (excluding cycle 257 where this trend was not detected) (Fig. 7). *Coccolithus pelagicus* is present with abundances lower than 7% in the sapropels and is almost absent in the marly limestone/marlstone layers (Fig. 7). The abundance of reworked specimens generally does not exceed 5% (Fig. 7).

4.4. Environmental indexes and statistical analysis

The W-O/C-E trend shows a consistent pattern, with W—O taxa as dominant in the sapropel and C-E in the marly limestone/marlstone (Fig. 8). This pattern is less clear in cycle 253, where prominent

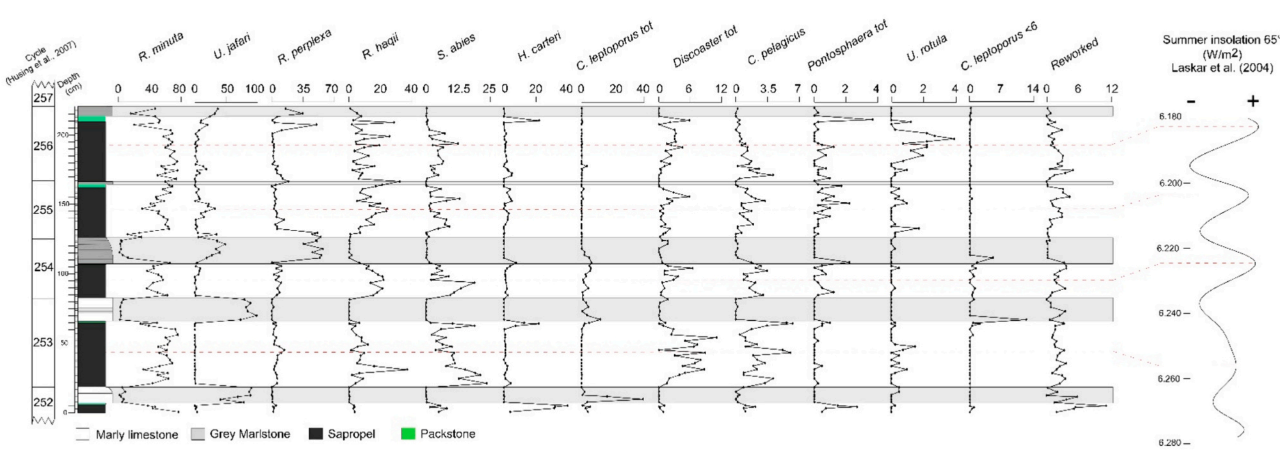

Fig. 7. Calcareous nannofossil relative abundance in relation to the summer insolation at 65°N (Laskar et al., 2004). The horizontal dotted red line indicates the sapropel mid-point. (For interpretation of the references to colour in this figure legend, the reader is referred to the web version of this article.)

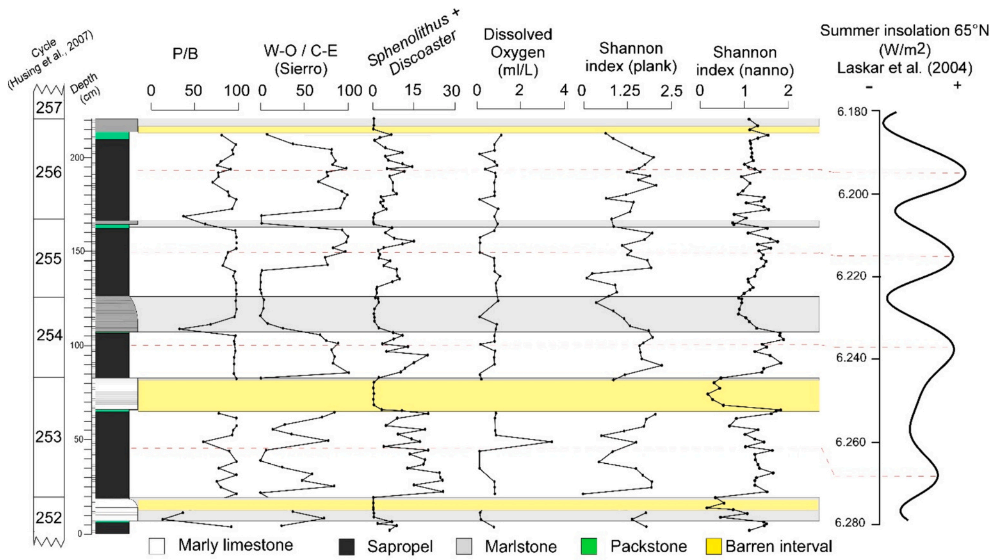

Fig. 8. Paleoenvironmental and statistical indexes calculated on the micropaleontological content. For detail refer to 2.2, 2.3 and 2.4.

fluctuations of foraminifer taxa are recorded. The calculated P/B ratio exhibits high values in the sapropel and generally low values in the marly limestone samples, except at the top of cycle 254 where the values are comparable to the sapropel samples (Fig. 8). The dissolved oxygen index exhibits value from 0 to 3.4 mL/L with no clear correlation with the lithology (Fig. 8). The warm water taxa *Discoaster* spp. and *Sphenolithus* spp. show high abundance in the sapropel layers, especially in cycle 253.

The PCA result was obtained for CN and PF separately and the results are shown in Fig. 9; two principal components explain the 34.1% - 48.6% of the variance recorded (Fig. 9). For calcareous nannofossil, the highest positive loading with PC1 is reached by *R. minuta*, *C. pelagicus* and *Sphenolithus* gr. (0.4, 0.27 and 0.26, respectively), while the higher negative loading is shown by *U. Jafari* and *R. perplexa* (0.42 and 0.31, respectively). The highest loading for PC2 is reached by *Discoaster* gr and *U. rotula* (0.27), while negative loading is shown by *H. carteri*, *Pontosphaera* gr and *S. pulchra* (−0.4, −0.4 and − 3.6, respectively) (Fig. 9). Based on the distribution of the taxa and considering their known paleoecological requirements, we extrapolated the most likely environmental parameter controlling the PCs. We used as end members the paleoecology of *S. abies*, *Discoaster*, *H. carteri* according to Corselli et al. (2002), Ziveri et al. (2004), Flores et al. (2005) and Mancini et al. (2020) to constrain the PC1 and PC2 as mostly controlled by SST and Sea Surface Salinity (SSS), respectively (Fig. 9). It is important to consider that these environmental variables are related to other parameters, for instance the SST encloses information also on the stability of the water column (stratification vs turbulence) and on primary productivity features (high SST usually results in stratified water column with surface oligotrophy and eventually DCM formation; low SST favors water turbulence and mixing of nutrients, which stimulate primary productivity). According to the PCA results, the taxa are distributed in 4 distinct groups: group 1 and 2 represent the taxa dominating in the marly limestone/marlstone and the sapropel samples, respectively (Fig. 9); group 4 represents the taxa dominating the packstone layer, while group 3 grouped the taxa with intermediate abundance recorded in the sapropel samples.

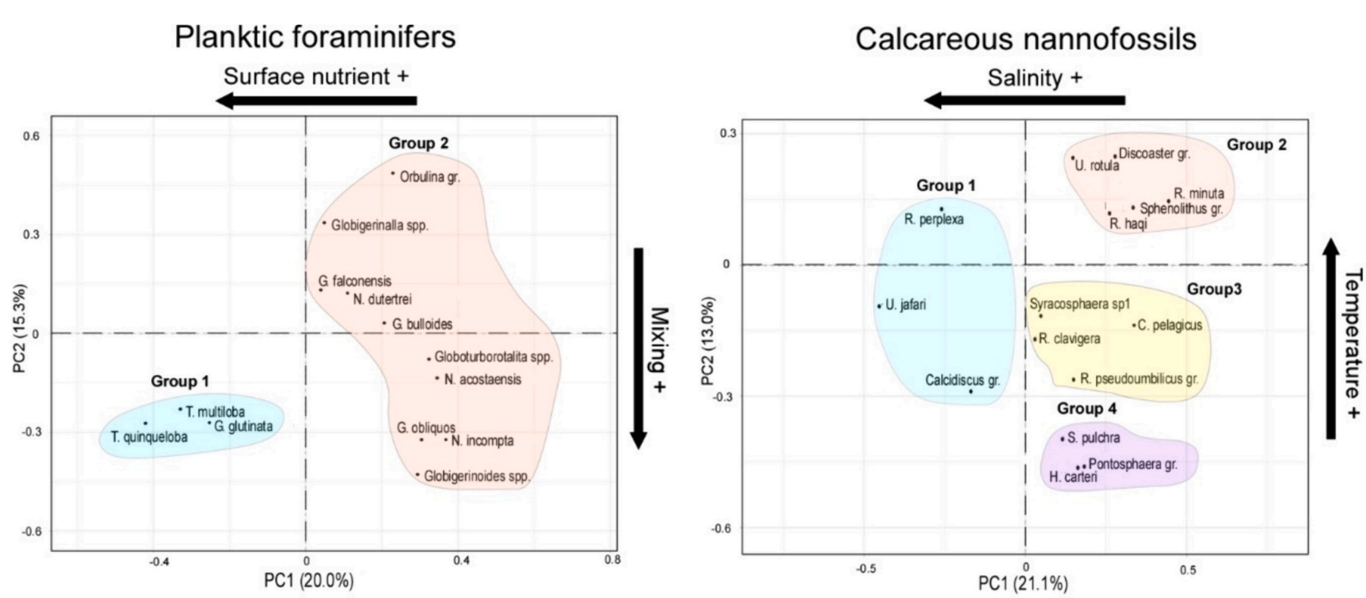

Fig. 9. Principal Component Analysis results of the calcareous nannofossil and planktic foraminifer relative abundance.
The constraining of the environmental variable driving PC1 and PC2 are introduced and discussed in paragraphs 4.4.

For the planktic foraminifer, along PC1, *T. quinqueloba*, *T. multiloba*, and *G. glutinata* are aggregated as group 1 and separated from the other taxa, showing the highest negative loading (−0.42, −0.32 and − 0.25, respectively) (Fig. 9). Therefore, PC1 could be representative of surface primary productivity controlled by nutrient availability, as these taxa thrive in these types of marine conditions (Volkmann, 2000; Schiebel et al., 2001; Riforgiato et al., 2008; Schiebel and Hemleben, 2017). Group 1 represents the taxa preferentially recorded in the marly limestone/marlstone layers, while group 2 the taxa recorded in the sapropels. The PC2 shows the highest positive loading with *Orbulina* gr. and *Globigerinella* spp. (0.48 and 0.38), while negative loading are recorded for *Globigerinoides* spp., *N. incompta* and *G. obliquos* (−0.43, −0.35 and − 0.35, respectively) (Fig. 9). Reconstructing the environmental parameter predominantly influencing PC2 is not straightforward due to the complexity associated with group 2. This group, aligned with PC2, comprises taxa with well-documented yet contrasting ecological requirements. Therefore, we speculate that the most probable environmental variable is the mixing of the upper water column, as recently reconstructed by Azibeiro et al. (2023) through the study of the Mediterranean surface sediments.

5. Discussion

5.1. Age model

The studied section corresponds to a portion documented in Hüsing et al. (2009), in Fig. 2A and C). The sampled cycles correspond to cycles 252–257, with an inferred age spanning from 6.56 to 6.48 Ma (Hüsing et al., 2009). The age model provided by Hüsing et al. (2009) relies on planktic foraminifer bioevents reported by Sierro et al. (2001), which are thought to be synchronous in the whole Mediterranean. However, differently from the results reported by Hüsing et al. (2009), our planktic foraminifer analysis also shows the presence of *Turborotalita multiloba*, whose first abundant peak is a bioevent largely applied and dated at 6.413 Ma. This implies that the studied sediments are younger than the age reported by Hüsing et al. (2009), who dated the cycles under examination between 6.553 Ma (precession maxima in the limestone of cycle 253) to 6.480 Ma (precession maxima in the limestone of cycle 257). *Turborotalita multiloba* was also recorded by Montanari et al. (1995) by studying the same succession but in an outcrop on the top of the Monte dei Corvi cliff. The inconsistency with the age model of Hüsing et al. (2009) is probably due to their lower sampling resolution compared to our study and the very short duration of the *T. multiloba* peaks. Indeed, Hüsing et al. (2009) performed semi-quantitative analysis on 70 samples on ~40 m of section, while we performed 66 quantitative analysis over ~3 m. In addition, Other planktic foraminifer taxa can be used to refine the age model of the studied sediments: 1) the absence of *Globorotalia scitula* (which shows two influxes after the FCO of T. *multiloba* at 6.285 and 6.098 Ma, respectively), 2) the prevalence of right coiled *N. acostaensis* and the occurrence of T. *multiloba* peaks in cycles 254, 255 and 256. These suggest the correlation with cycles UA21 to UA25 of the Perales section (Sorbas Basin, Spain; Sierro et al., 2001), therefore refining the age of the studied interval between 6.275 and 6.184 Ma (Fig. 4). This hypothesis is also corroborated by the thickness of the cycle 253, which as in the case of Perales section, is thicker than the others and corresponds to a period of eccentricity minimum lacking a prominent low insolation phase.

Moreover, our results suggest that high-resolution studies can improve the age model of Messinian key sections, as some planktic foraminifer-based bioevents can be short-living, especially in those sections characterized by a low sedimentation rate.

5.2. Depositional setting of Monte dei Corvi section

The cyclicity expressed by the micropaleontological assemblages, which is in phase with precessional variations is the most evident characteristic of the studied succession: a pattern commonly observed in Messinian pre-evaporitic sediments (Sierro et al., 2003; Lozar et al., 2018; Gennari et al., 2018; Gennari et al., 2020; Mancini et al., 2021; Tzevahirtzian et al., 2023; Gennari et al., 2024; Bertini et al., 2024). The absence of bioturbation in the sapropel layers associated with the presence of pyrite (Fig. 3), and the presence of scattered benthic foraminifer known to thrive in conditions of high carbon rain and low oxygen, such as *bolivinids*, *buliminids*, and *uvigerinids* (Jannink et al., 1998; Murray, 2006) marks sea bottom deoxygenation, or even anoxic condition, as suggested by the dissolved oxygen index (Fig. 8).

The above-mentioned benthic foraminifer taxa have the capability to utilize nitrogen, rather than oxygen, as an electron acceptor for respiration (Glock et al., 2019). This capacity may elucidate the coexistence of benthic foraminifer alongside the absence of bioturbation, a phenomenon typically linked with organisms reliant on oxygen. The relatively high abundance of benthic taxa indicative of an oxygenated environment in the sapropel layers (i.e. *Lobatula lobatula*, *Elphidium* spp. and *Porosononion granosum*) is at odds with the reconstructed anoxic condition and depositional setting; in fact, based on the mollusk content Iaccarino et al. (2008) suggested an outer shelf/upper slope depositional environment (200–600 m;), while these taxa are classified as oxygenated inner shelf inhabitants (Van der Zwaan et al., 1990; Murray, 2006). Therefore, we suggest that these taxa were reworked or displaced from marginal areas. It is noteworthy that specific samples of marly limestone/marlstone (Fig. 8) exhibit dissolved oxygen values indicative of hypoxic conditions (< 2 mL/L), and in some instances, even reaching anoxia. This seems contradictory as these layers are supposed to form during insolation minima, when the water column was well mixed; however, rather than stratification, low oxygen conditions during the deposition of these layers may have been triggered by high export production. Considering the presence of scattered bioturbation in these layers (Mancini et al., 2024a) it can be speculated that the high productivity and low oxygen sea floor were not permanently established but were seasonal or alternated with periods of lower export and ventilated bottom waters. The Monte dei Corvi section records cyclical deoxygenation events in the deep Adriatic setting, and this is believed to reflect variations in the ADW formation system in phase with the precessional forcing (Mancini et al., 2024a). According to this view, the packstone and sapropel layers would represent the maximum and minimum strength, respectively, of intermediate to deep water flowing along the external Adriatic foredeep.

5.2.1. Sapropel depositional mechanism

High diversity of planktic foraminifer and nannofossils, evidenced by the Shannon index, characterizes the sapropel layers (Fig. 8). Both groups typically exhibit greater diversity in warm, stratified, and oligotrophic regions, such as subtropical gyres (Winter, 1994; Baumann et al., 2005; Schiebel and Hemleben, 2017). In detail, the sapropels are characterized by higher W-O/C-E index (Fig. 8) due to the abundance of *Orbulina* spp., *Globoturborotalita* spp. and Neogloboquadrinids (Fig. 5), along with *Discoaster* spp. and *S. abies* among the calcareous nannofossils (Fig. 7). While *Orbulina* spp. and the *Globoturborotalita* gr. are adapted to warm and oligotrophic surface conditions, the Neogloboquadrinids are commonly associated with the formation of a Deep Chlorophyll Maximum (DCM) (Sierro et al., 2003). Neogloboquadrinids are generally absent in Messinian sapropels (Blanchet et al., 2021; Sierro et al., 2003; Gennari et al., 2018; Gennari et al., 2023) probably due to warm SST (Sierro et al., 2003). Therefore, their presence in the northern paleo-Adriatic basin during sapropel deposition may indicate winter SST lower than 14 °C (Sierro et al., 2003, based on the database of Kallel et al., 1997). Among calcareous nannofossil, the presence of *Discoaster* spp. and *S. abies*, which are both inhabitants of the middle to lower photic zone and able to flourish in warm and stratified water (Gibbs et al., 2004; Flores et al., 2005; Mancini et al., 2020) suggests the occurrence of a DCM, a condition typically associated with vertical stratification of the water column. The presence of a DCM can significantly increase the organic carbon deposited at the sea bottom, as organic matter bypasses remineralization in the upper photic zone, where organic carbon degradation rates are higher (Fig. 10; De La Rocha and Passow, 2007). This not only has local consequences on the organic carbon storage in sediments, but can have larger impacts, as it has been estimated that a 24-m increase in the depth at which 63% of sinking carbon is respired results in a decrease of atmospheric CO_2 concentrations by 10–27 ppm (Kwon et al., 2009). In essence, the presence of a DCM alone can influence remineralization rates across the entire water column, increase the organic rain to the sea floor and affect bottom oxygen levels. In the Messinian paleo-Adriatic basin, the DCM was favored by warming and freshening of surface waters, which reduced the strength of the thermohaline circulation due to the buoyancy gain of surface water (Fig. 10). The DCM is a common feature reported from the analysis of Quaternary and Neogene sapropels (Castradori, 1998; Rohling et al., 2015; Mancini et al., 2024b). This presence is often associated with enhanced continental runoff delivering nutrients, primarily from the Nile River (Rohling et al., 2015). However, in our case, the W-O/C-E index suggests lower surface primary productivity in the sapropels compared to other layers (see Fig. 8). Therefore, we propose that bottom water deoxygenation in the sapropel layers was more likely related to the warming and freshening of the water column and its biogeochemical

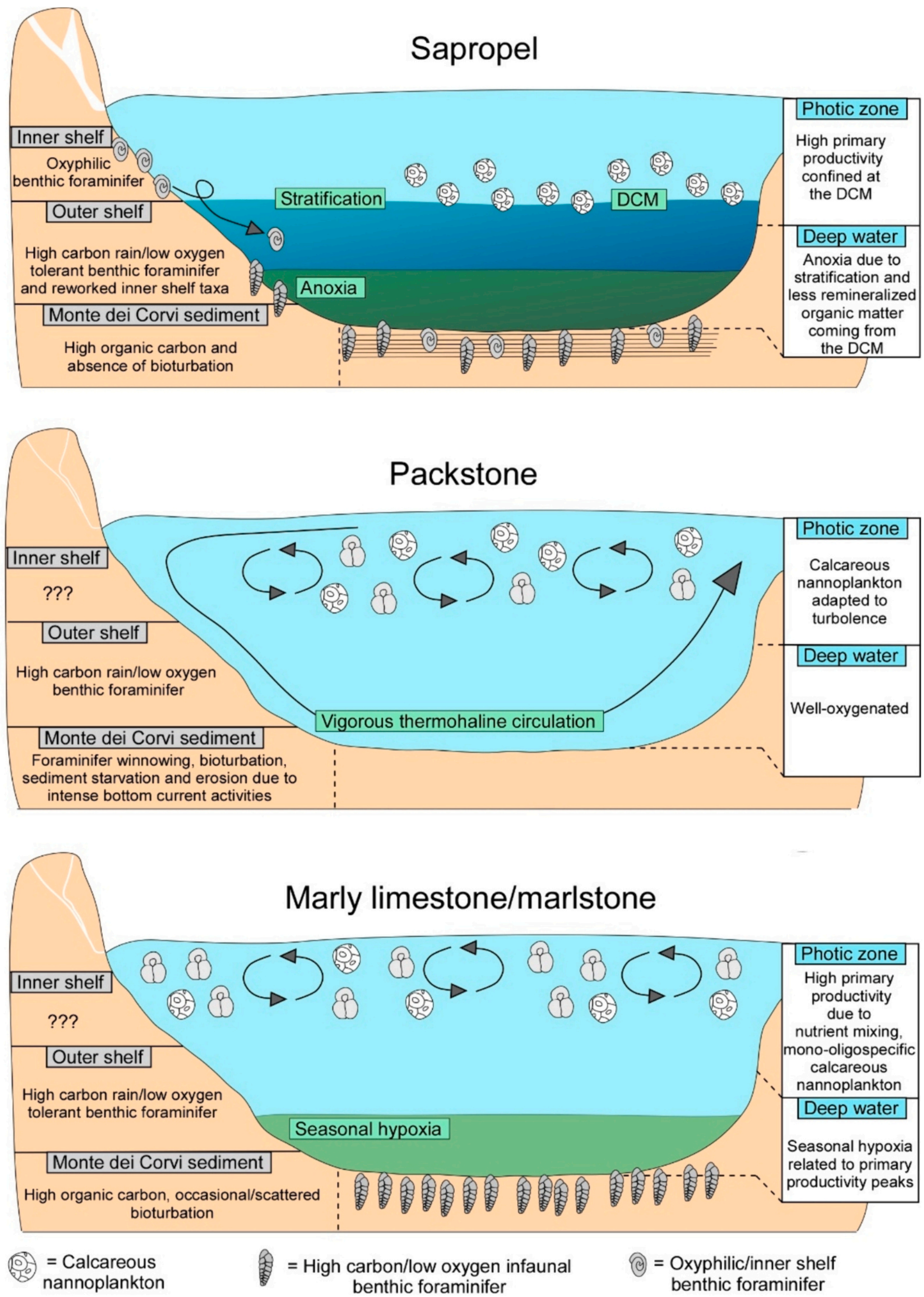

Fig. 10. Sketch showing the oceanographic and biological processes characterizing the deposition of the different lithologies as reconstructed in paragraph 5.1.

structure (i.e., the presence of a DCM) and not to the overall amount of primary productivity generated (Fig. 10). Enhanced freshwater input during the sapropel deposition is also documented by the relatively high presence of benthic inner shelf taxa (Fig. 6), which were probably reworked from marginal areas. Sustained continental runoff is also documented by the high amount of terrigenous in the sapropel, recorded either with X-ray diffractometry (Mancini et al., 2024a) and through EDS or morphological inspection (Fig. 3). We may speculate that such continental runoff may have generated by local rivers in the emerging Apennines chain or in the Alps (Ghielmi et al., 2010; Sabino et al., 2020; Bertini et al., 2024) but also by African rivers, as during the Messinian, freshwater discharge was three times greater than present-day conditions in the Mediterranean (Gladstone et al., 2007; Simon et al., 2017). Alternatively, the freshwater inflow from the Paratethys (Gladstone et al., 2007; Vasiliev et al., 2019; Grothe et al., 2020; Krijgsman et al., 2020) cannot be ruled out. Nevertheless, the freshwater discharge during the Messinian occurred during a "warmer than present" interval (see 5.2 paragraph), which further facilitated the density loss of surface water thus impacting the thermohaline circulation strength. Our data further confirm that during the sapropel deposition the ADW formation was diminished or blocked, as testified by foraminifer and calcareous nannofossils content. However, the ADW formation depends also on the formation rate and physical characteristics of the LIW, which influence the circulation and oxygenation of bottom water. Future efforts may be addressed to disentangle the LIW influence on the ADW formation and bottom oxygenation.

5.2.2. Packstone and marly limestone/marlstone depositional mechanism

Both packstone and marly limestone/marlstone layers exhibit distinct micropaleontological assemblages. Among calcareous nannofossils, the transitions from sapropel to packstones show pronounced peaks of *H. carteri* and *Pontosphaera* spp., followed by peaks of *C. leptoporus* (except in cycle 257) (Fig. 7). Subsequently, the marly limestone/marlstone layers are characterized by either oligospecific or monospecific assemblages, primarily composed of *U. jafari* and *R. perplexa* (Fig. 7). *Helicosphaera carteri* is a living taxon known to thrive in environments marked by salinity fluctuations, mesotrophy, and turbid waters (Giraudeau, 1992; Corselli et al., 2002; Ziveri et al., 2004; Bonomo et al., 2021). Its resilience to water turbulence is evidenced by its presence in upwelling settings (Ziveri et al., 2004). Similarly, *Pontosphaera* spp. are abundant in shelf settings (Perch-Nielsen, 1985; Bown and Young, 2019), indicating their ability to tolerate water turbulence and salinity fluctuations (Lozar et al., 2010). Collectively, these two taxa suggest mixing of the upper water column. Overall, the high abundance of *C. leptoporus* in modern oceans is primarily found in temperate to subpolar regions characterized by eutrophic conditions and upwelling (Renaud et al., 2002; Boeckel and Baumann, 2004; Ziveri et al., 2004). Although cementation of some marly limestone samples (paragraph 3.2) hindered the extraction of foraminifer from the bulk rock, the available data indicate that *T. multiloba* and *T. quinqueloba* dominate these layers, along with a high abundance of *Bolivina* spp. and *Bulimina* spp. (Figs. 4 and 5). *Turborotalita quinqueloba* is a living taxon, thriving in cold and eutrophic waters (Hemleben et al., 1989; Sierro et al., 2003; Schiebel and Hemleben, 2017). The high abundance of *Bolivina* spp. and *Bulimina* spp. among the benthic foraminifer (Fig. 6) suggests significant carbon deposition on the seafloor, indicative of eutrophication of the upper water column and hypoxic condition at the sea bottom, a condition also confirmed by the scarce bioturbation. Noteworthy, in these intervals the inner shelf foraminifer decrease (Fig. 6) suggesting decreased runoff. Instead, an erosional surface occurring at the base of the packstone layer was probably caused by the action of the dense water formation in the Northern Adriatic, which in modern setting flows Southward at 50–150 m (Artegiani et al., 1997). This ADW-related current caused a sedimentary hiatus (Mancini et al., 2024a), hindering the determination of the exact timing of deep basin re-oxygenation. Despite this, our micropaleontological data suggest that the sapropel-packstone transition reflects the disruption of stratification caused by increased water mixing and turbulence, in turn increasing primary productivity. The stimulation of primary productivity in the upper photic zone might be the response to surface water density changes resulting from increasing salinity and/or cooling of surface waters, which distribute the nutrient through mixing (Fig. 10). This micropaleontological content aligns with previous studies (Bertini, 2006; Iaccarino et al., 2008; Di Stefano et al., 2010; Mancini et al., 2024a) that indicated higher salinity and increased surface water density at the time of marly limestone/marlstone deposition. Therefore, increased export following enhanced productivity was likely responsible for the hypoxic conditions at the bottom during the marly limestone/marlstone deposition.

5.2.3. Deciphering the significance of oligo/monospecific calcareous nannofossil assemblages in the marly limestone/marlstone

The occurrence of monospecific and/or oligospecific assemblages of *U. jafari* in some marly limestone/marlstone layers (see Figs. 2 and 6) is noteworthy. Selective dissolution is not the cause of the high concentration of this taxon, as *U. jafari* is known to be dissolution-prone (Gibbs et al., 2004). In addition, *U. jafari* coccoliths are found closely embedded in well-preserved fecal pellets (Fig. 3), further suggesting their pristine signal from the upper water column rather than a diagenetic process at the bottom. *Umbilicosphaera jafari* has been widely documented in both pre-evaporitic and evaporitic sediments occurring in the Messinian (Flores et al., 2005; Wade and Bown, 2006; Di Stefano et al., 2010; Lozar et al., 2018; Gennari et al., 2018; Mancini et al., 2022). Its behavior during the Messinian is distinctive, displaying prominent and typically short-lived fluctuations where it tends to dominate the assemblage, often replacing small reticulofenestrids (*R. minuta*), with percentages ranging from 50% to 90% (Flores et al., 2005; Wade and Bown, 2006; Di Stefano et al., 2010; Lozar et al., 2018; Gennari et al., 2018; Pellegrino et al., 2020; Mancini et al., 2020; Gennari et al., 2023). This behavior suggests an r-strategy, making this taxon opportunistic for specific environmental conditions. Previous studies indicated that during the Messinian, *U. jafari* abundance fluctuated in response to precessional variations, with maximum values during precession maxima (insolation minima) (Lozar et al., 2018; Gennari et al., 2018). Finally, *U. jafari* was usually associated with restricted environments and/or high salinity and cold conditions (Flores et al., 2005; Wade and Bown, 2006; Di Stefano et al., 2010; Lozar et al., 2018; Gennari et al., 2018). Based on i) the highest abundance of *U. jafari* associated with rather high salinity (> 37‰) (Mancini et al., 2024a), ii) the presence of high amounts of fecal pellets made of monospecific *U. jafari* assemblage (Fig. 3), and iii) *U. jafari* peaks being correlated with high benthic foraminifer abundance, indicative of high organic carbon deposition on the seafloor, and with the eutrophic taxa *T. multiloba* and *T. quinqueloba*, we suggest that at the Monte dei Corvi section, the high abundance of *U. jafari* is related to slightly elevated salinity and eutrophication of the upper water column (Fig. 10). Interestingly, this taxon was found associated with *C. leptoporus* in the Tokhni section (Cyprus) during insolation minima (Gennari et al., 2018) from ~6.4 to 6.1 Ma. Similarly to our record, at Tokhni the *U. jafari* is then replaced by *R. perplexa*. Indeed, in cycles 255, 256, and 257, *U. jafari* is accompanied or replaced by *R. perplexa* (Fig. 7). Furthermore, the planktic and benthic foraminifer assemblages associated with *R. perplexa* are similar to those associated with *U. jafari*, suggesting similar paleoecological requirements. Our PCA analysis suggests the association of *R. perplexa* with less saline and warmer surface waters compared to *U. Jafari* (Fig. 9). Finally, *R. perplexa* peaks are also associated with a higher diversity of the assemblage, as indicated by the Shannon index (Fig. 8), suggesting less harsh and more stable environmental conditions.

5.3. Snapshot on the Messinian surface water and comparison with present-day

Our analysis points to alternating conditions of stagnation and low productivity (sapropels) that switch to well-mixed with high productivity (packstone/marly limestone). Similar reconstructions were achieved in other pre-evaporitic Messinian successions (Sierro et al., 2003; Kouwenhoven and Van der Zwaan, 2006; Riforgiato et al., 2008; Lozar et al., 2018; Gennari et al., 2018; Gennari et al., 2023; Bertini et al., 2024). During the Messinian, the SSTs were higher than the modern conditions and probably matched those predicted at the end of this century under the business-as-usual scenario (Mancini et al., 2024a). For the analyzed time interval, Mayser et al. (2017) reported Tex_{86}-based SST spanning 25.1–28.9 °C in Cyprus, and Tzanova et al. (2015) reported alkenone-based SST from 24 to 26 °C in the Monte dei Corvi. Hence, the Messinian interval can serve as an analog of a "warmer than present" Mediterranean, offering the potential to anticipate its response to ongoing climate change. With this in mind, we compiled the foraminifer dataset spanning the 6.28–6.18 Ma time interval in different localities of the major sub-basins of the Mediterranean (Fig. 11). For each locality, we averaged the relative abundance of the major taxa during this 100 ka time interval (Fig. 11). The mean values obtained were then compared to the dataset of Azibeiro et al. (2023), that shows a snapshot of the modern planktic foraminifer assemblage recorded in surface sediment of the Mediterranean. We acknowledge that Azibeiro et al. (2023) considered the >150 μm size fraction of the washed residues, artificially diminishing the abundance of smaller taxa (e.g., *T. quinqueloba*). It is noteworthy that the standard fraction utilized in Messinian studies is the >125 μm, except Sierro et al. (2003), who utilized >150 μm. Furthermore, in Azibeiro et al. (2023) the planktic foraminifer record of the Northern Adriatic is not reported and finally, the analysis was performed on surface sediments, which most probably represents an average of less than ~100 years, while our dataset spans 100 ka. Despite these differences, the comparison that we propose is used to roughly discriminate the main oceanographic features characterizing the two different time windows. Azibeiro et al. (2023) underline that the zonal distribution and the meridional gradient of planktic foraminifer assemblage are primarily related to productivity, rather than SST. These changes in productivity are statistically explained by the nutrient content of the deep water and by the capacity of this water to uplift, the latter driven by regional hydrography (Azibeiro et al., 2023).

The first prominent difference is the *Globigerinoides* abundance (*Globigerinoides ruber* in Azibeiro et al., 2023; *Globigerinoides* spp. in our work), which in the modern setting is dominant (up to 80%) in the Eastern Mediterranean, while during the Messinian it was dominant in the Western Mediterranean (Fig. 11). Furthermore, looking at the W—O taxa (*Globoturborotalita, Orbulina, Globigerinoides* and *Globigerinella*) it results that the Western and Northern Mediterranean were probably warmer than the modern setting, which shows the highest abundance of these taxa in the Levantine Basin (Azibeiro et al., 2023), which is indeed the warmer part of the Mediterranean today.

Except for the Pissouri and Sorbas cases, *T. quinqueloba* dominates the Messinian planktic foraminifer assemblage (14–30%), with the highest abundance in the Aegean Sea (Gavdos section, Fig. 11D). In contrast, *T. quinqueloba* abundance in the present-day Mediterranean never exceed 5%, with the highest values reported in the inner Aegean Sea, the Thyrrenian and the Balearic Seas (Azibeiro et al., 2023). The difference in the *T. quinqueloba* absolute abundance can be ascribed to different primary productivity regimes, which were higher during the Messinian, probably because the freshwater input delivering nutrients from African rivers in the Eastern Mediterranean was enhanced (Gladstone et al., 2007; Simon et al., 2017).

Also, the Neogloboquadrinids record (*N. pachyderma* and *N. incompta* in Azibeiro et al., 2023) in the present-day setting is high only in the Gulf of Lion and in the Eastern Balearic Sea (up to 70%), while scattered or even absent in the rest of the Mediterranean (Azibeiro et al., 2023). Neogloboquadrinids are categorized as C-E (Sierro et al., 2003; Schiebel and Hemleben, 2017), but they are also referred to be active predators at the DCM, a condition usually related to stratification of the water column. According to Kallel et al. (1997), Sierro et al., 2003, Azibeiro et al. (2023), Neogloboquadrinids in the Mediterranean are probably restricted to certain SST thresholds: spring SST between 6 °C - 14 °C and winter SST below 14 °C. Our compilation for the Messinian shows the highest abundance of Neogloboquadrinids in the Levantine Sea (Fig. 11E) which may highlight either enhanced stratification, relatively cold SST, or sustained primary productivity. Since the

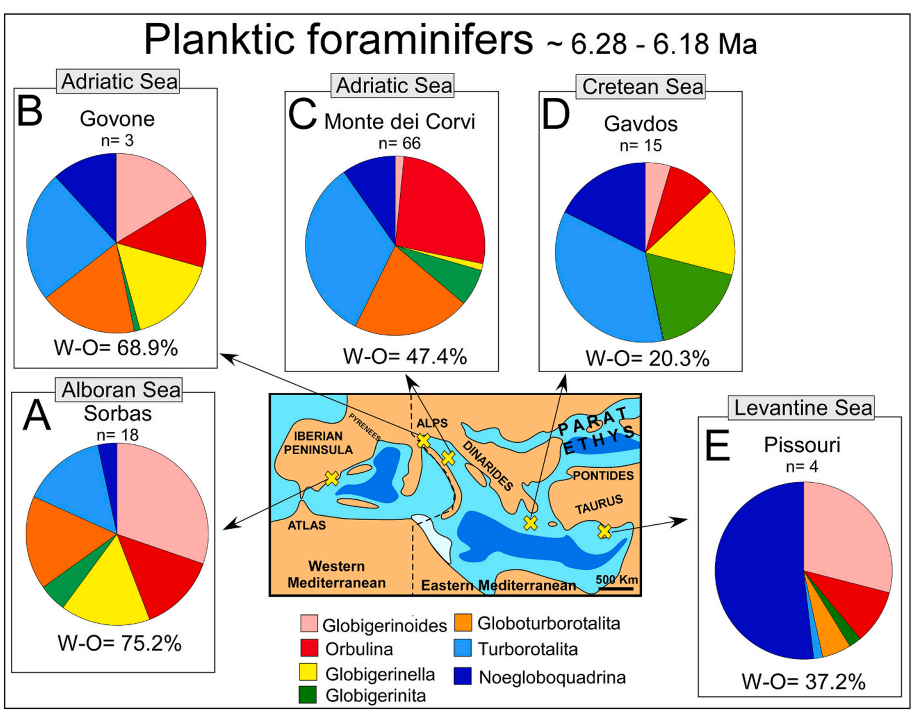

Fig. 11. Planktic foraminifer assemblage averaged from 6.28 to 6.18 Ma in different sites: Sorbas (Sierro et al., 2003; Mancini et al., 2020. Alboran Sea); Govone (Gennari et al., 2020. Adriatic Sea); Monte dei Corvi (this work. Adriatic Sea); Gavdos (Gennari et al., 2023. Cretan Sea); Pissouri (Kouwenhoven and Van der Zwaan, 2006. Levantine Sea).

Neogloboquadrinids record in the Levantine Sea is not associated with elevated W—O foraminifer taxa (Fig. 11E), but alkenone-based SST reconstruction indicates warm conditions (22 °C – 29.8 °C; Mayser et al., 2017) it is possible that eutrophication masked the W—O signal. Indeed, the distribution of planktic foraminifer in the Mediterranean mostly follows nutrient availability (productivity regime), rather than SST (Azibeiro et al., 2023), also matching our reconstruction of PC in the PCA analysis (Fig. 9). During the Messinian, the nutrients likely entered the Eastern Mediterranean through African rivers, which stimulated primary productivity and enhanced stratification, both conditions adequate for Neogloboquadrinids proliferation.

Other possible sources of nutrients were influxes from the Paratethys and rivers entering the Mediterranean from its northern border (Gladstone et al., 2007; Simon et al., 2017; Vasiliev et al., 2019; Grothe et al., 2020; Krijgsman et al., 2020; Sabino et al., 2020; Gennari et al., 2024; Bertini et al., 2024). This suggests that eutrophication characterizing the Messinian was the main responsible for the difference in the planktic foraminifer record with the contemporary setting. The Neogloboquadrinids are important components of the Messinian assemblage in the Adriatic and Aegean seas (Fig. 9B and C), suggesting more freshwater influence compared to present-day conditions in these areas (Gladstone et al., 2007; Simon et al., 2017).

As for the Gavdos section, which recorded the dynamic of the Cretan sea (Fig. 11), the Messinian assemblage was different compared with today (Fig. 11D; Azibeiro et al., 2023), showing low abundance of W—O taxa (20.3% compared to 60–90% in the present-day setting). Similarly to the Levantine case (Fig. 11E), the reconstructed SST (27.2 °C – 30 °C; Kontakiotis et al., 2022) is at odds with a scarce abundance of W—O taxa, further suggesting that the C-E overwhelms the W—O signal because of enhanced primary productivity not associated with cooling.

Finally, moving westward, the present-day Alboran Sea, is dominated by the cold eutrophic *Globoconella inflata* and *G. bulloides* (up to 50%) and to a lesser extent, by the ubiquitous *G. glutinata* (4% - 10%) (Azibeiro et al., 2023). In addition, *G. glutinata* shows the highest abundance in subtropical or temperate water during seasons characterized by nutrient enrichment and phytoplankton bloom (Schiebel et al., 2001; Schiebel and Hemleben, 2017). All the mentioned taxa rely on the relatively nutrient-enriched water entering the Mediterranean through Gibraltar (Azibeiro et al., 2023). In contrast, the Messinian Sorbas Basin, which represents the Northern Alboran Sea, shows the highest W—O abundance (Fig. 11A), significantly differing from the present-day record. Therefore, we suggest a lower marine productivity regime in the Sorbas Basin compared to the Eastern Mediterranean, probably due to lower continental runoff as the African rivers and Parathetys inflow did not reach this part of the basin. This also suggests that contrarily to the modern situation (Schroeder et al., 2023), the water inflow from the Atlantic was nutrient-depleted compared with the Mediterranean water.

Collectively, our analysis argues for an overall eutrophic environment for the Messinian, especially in the Eastern Mediterranean, evidencing that the paleo-Mediterranean significantly differs from the contemporary setting, which is, overall, oligotrophic and ultra-oligotrophic.

5.4. Factors influencing the Messinian oxygen balance: lessons for unraveling future trends

Literature data document that the Mediterranean Sea during the Messinian was characterized by elevated SST (Tzanova et al., 2015; Mayser et al., 2017; Vasiliev et al., 2019; Kontakiotis et al., 2022), which likely decreased the oxygen solubility of the seawater, increased the biological metabolism and the consequent oxygen consumption, and increased the stratification potential of the water column (decrease in the thermohaline circulation). Other crucial characteristics of the Messinian were the restricted exchange with the Atlantic and the sustained runoff (Gladstone et al., 2007; Simon et al., 2017; Corbí et al., 2020), which further diminished the bottom oxygen through the stimulation of primary productivity, and through decreasing the surface density of water, which inhibited vertical advection and the consequent oxygen delivery at the bottom. Moreover, the restricted condition characterizing the Messinian weakened the Mediterranean outflow in the Atlantic (Bulian et al., 2023), likely enriching the nutrient content of bottom water of the Mediterranean. If the nutrient-enriched bottom water were to upwell, it would have boosted primary productivity. This could have been an additional mechanism, together with the increased nutrient-delivered runoff, for the observed enhanced productivity during the Messinian. Therefore, the Mediterranean Sea during the Messinian satisfied the major requirement for widespread and protracted deoxygenation events: elevated SST, productivity and runoff. We also showed that with relatively high SST (higher than present-day) and primary productivity, but with decreasing runoff and the associated stratification of the water column, bottom hypoxic conditions are achieved and poorly laminated marlstone and marly limestone are deposited (paragraph 5.1.2). Insights obtained from this record contribute to our understanding of potential future events that may impact the Mediterranean area. The Messinian lesson teaches us that, identifying the key factors influencing bottom oxygen balance is instrumental in undertaking tasks related to mitigation and adaptation strategies.

If we consider the present-day Mediterranean Sea, we are aware that the bottom oxygen balance varies in function of seawater temperature, the density of the water column and primary productivity-consumption pattern (Altieri and Gedan, 2015; Limburg et al., 2020). In particular, the Mediterranean area is sensitive to oxygen starvation conditions, especially in the coastal and marginal areas where the influence of continental runoff delivering nutrients stimulates primary productivity (UNEP, 1996; Turley, 1999; Stachowitsch et al., 2012; Viaroli et al., 2015; Mancini et al., 2024b). Furthermore, the ongoing climate change is pushing down the Mediterranean oxygen inventory (Somot et al., 2006; Reale et al., 2022), therefore impacting the marine biota. Also, despite the Mediterranean currently experiencing warming, continental runoff is not increasing; instead, it is decreasing due to reduced rainfall (Somot et al., 2006; Sanchez-Gomez et al., 2009; MedECC, 2020; Reale et al., 2022). Moreover, the water exchange with the Atlantic in the present-day Mediterranean is not as restricted as during the Messinian (Flecker et al., 2015), therefore the nutrient enrichment provided by continental runoff is expected to be minor when compared to the Messinian conditions. However, while the contemporary Mediterranean experiences a decrease in continental runoff, rivers transport anthropogenically enriched nutrients (Diaz and Rosenberg, 2008), potentially mitigating the reduction in nutrient availability resulting from decreased continental runoff. The precise recognition of the future oxygen balance in response to changing conditions is hampered by the considerable uncertainty surrounding the projections for primary productivity in the open Mediterranean Sea setting for the end of this century under a "business-as-usual" scenario. Studies have suggested a decrease (Richon et al., 2019), stability (Macias et al., 2015), and an increase (Lazzari et al., 2014). But the geological record indicates that deoxygenation events are closely associated with rapid warming periods (Foster et al., 2018; Mancini et al., 2024b). The Messinian record further shows that bottom hypoxic conditions are established even with declining runoff, as long as primary productivity is high.

Considering the rapid warming of the Mediterranean region, there are growing concerns about significant deoxygenation in the future. This concern becomes particularly pronounced when coupled with sustained primary productivity, as seen during the deposition of marly limestone at Monte dei Corvi. This highlights the importance of surface primary productivity for the bottom oxygen inventory. Based on this lesson, we suggest focusing on primary production as a key indicator to be monitored for understanding the future of this area.

6. Conclusion

The planktic and benthic assemblage recorded in the Monte dei Corvi section highlights cyclical deoxygenation dynamics related to the paleo ADW formation. These variations were driven by precessional fluctuation which controlled continental runoff and primary productivity regimes. The maximum decline in the ADW formation was related to increased runoff and low primary productivity, which resulted in bottom deoxygenation (down to anoxia) and sapropel deposition. The maximum strength of the ADW formation is recorded by the erosional surface at the sapropel-packstone layer transition. The establishment of bottom hypoxic condition, testified by poorly laminated marly limestone and its benthic foraminifer content, occurred with enhanced primary productivity but with decreased continental runoff. The increased marine productivity during this interval is also testified by the high abundance of fecal pellets composed of oligo-monospecific calcareous nannofossil assemblage.

The compilation of the existing microfossil datasets during the 6.28–6.18 Ma interval highlights important differences with the present-day distribution and abundance of planktic foraminifer, indicating a substantial difference in the two oceanographic settings. We suggest that this difference can be mostly ascribed to different productivity regimes, being the Messinian more eutrophic than the present-day Mediterranean. The increased susceptibility of the Mediterranean Sea to oxygen deficiency during the Messinian was related to the combination of warmer SST, enhanced stratification and primary productivity.

Currently, the Mediterranean is undergoing warming with declining continental runoff due to reduced rainfall. The future trend of primary production in this region remains uncertain, hindering precise predictions of the oxygen balance, yet insights from the Messinian period emphasize the critical role of primary productivity in shaping bottom oxygen conditions, highlighting the necessity for ongoing investigations.

CRediT authorship contribution statement

A.M. Mancini: Writing – review & editing, Writing – original draft, Visualization, Validation, Supervision, Project administration, Methodology, Investigation, Formal analysis, Data curation, Conceptualization. **S. Myers:** Writing – review & editing, Validation, Methodology, Investigation, Formal analysis, Data curation. **R. Gennari:** Writing – review & editing, Validation, Supervision, Methodology, Formal analysis, Conceptualization. **F. Lozar:** Writing – review & editing, Validation, Supervision, Project administration, Funding acquisition. **A. Negri:** Writing – review & editing, Validation, Supervision, Resources, Methodology, Funding acquisition, Conceptualization.

Declaration of competing interest

The authors declare the following financial interests/personal relationships which may be considered as potential competing interests.

Francesca Lozar reports financial support was provided by Cassa Risparmio Torino. If there are other authors, they declare that they have no known competing financial interests or personal relationships that could have appeared to influence the work reported in this paper.

Data availability

Data will be made available on request.

Acknowledgment

This project was supported by CRT (Cassa Risparmio Torino) grant 2021.0907 awarded to F.L and UNIVPM RSA 2024 to A.N. We acknowledge and thank the R/V Actea Captain Fabrizio Torsani for the help during the sampling operations. We thank Hugo Corbí and an anonymous reviewer for their smart comments and suggestions which improved the manuscript quality.

References

Altieri, A.H., Gedan, K.B., 2015. Climate change and dead zones. Glob. Chang. Biol. 21 (4), 1395–1406.
Artegiani, A., Paschini, E., Russo, A., Bregant, D., Raicich, F., Pinardi, N., 1997. The Adriatic Sea general circulation. Part II: baroclinic circulation structure. J. Phys. Oceanogr. 27 (8), 1515–1532.
Athanasiou, M., Triantaphyllou, M.V., Dimiza, M.D., Gogou, A., Panagiotopoulos, I., Arabas, A., Tsiolakis, E., 2021. Reconstruction of oceanographic and environmental conditions in the eastern Mediterranean (Kottafi Hill section, Cyprus Island) during the middle Miocene climate transition. Rev. Micropaleontol. 70, 100480.
Azibeiro, L.A., Kučera, M., Jonkers, L., Cloke-Hayes, A., Sierro, F.J., 2023. Nutrients and hydrography explain the composition of recent Mediterranean planktonic foraminiferal assemblages. Mar. Micropaleontol. 179, 102201.
Baumann, K.H., Andruleit, H., Böckel, B., Geisen, M., Kinkel, H., 2005. The significance of extant coccolithophores as indicators of ocean water masses, surface water temperature, and palaeoproductivity: a review. Paläontol. Z. 79, 93–112.
Bertini, A., 2006. The Northern Apennines palynological record as a contribute for the reconstruction of the Messinian palaeoenvironments. Sediment. Geol. 188, 235–258.
Bertini, A., Niccolini, G., Gennari, R., Lozar, F., Menichetti, E., Natalicchio, M., Pierre, F. D., 2024. Terrestrial and marine dynamics on the brink of the Messinian salinity crisis: a wet scenario from the northern Mediterranean. Glob. Planet. Chang. 104362.
Blanchet, C.L., Tjallingii, R., Schleicher, A.M., Schouten, S., Frank, M., Brauer, A., 2021. Deoxygenation dynamics on the western Nile deep-sea fan during sapropel S1 from seasonal to millennial timescales. Clim. Past 17 (3), 1025–1050.
Boeckel, B., Baumann, K.H., 2004. Distribution of coccoliths in surface sediments of the south-eastern South Atlantic Ocean: ecology, preservation and carbonate contribution. Mar. Micropaleontol. 51 (3–4), 301–320.
Bonomo, S., Schroeder, K., Cascella, A., Alberico, I., Lirer, F., 2021. Living coccolithophore communities in the Central Mediterranean Sea (Summer 2016): Relations between ecology and oceanography. Mar. Micropaleontol. 165, 101995.
Bown, P., Young, J., 2019. The fossil record of coastal coccolithophores. J. Nannoplankton Res. Sp 4, 73–80.
Breitburg, D., Levin, L.A., Oschlies, A., Grégoire, M., Chavez, F.P., Conley, D.J., Zhang, J., 2018. Declining oxygen in the global ocean and coastal waters. Science 359 (6371), eaam7240.
Bulian, F., Kouwenhoven, T.J., Jiménez-Espejo, F.J., Krijgsman, W., Andersen, N., Sierro, F.J., 2022. Impact of the Mediterranean-Atlantic connectivity and the late Miocene carbon shift on deep-sea communities in the Western Alboran Basin. Palaeogeogr. Palaeoclimatol. Palaeoecol. 589, 110841.
Bulian, F., Jiménez-Espejo, F.J., Andersen, N., Larrasoaña, J.C., Sierro, F.J., 2023. Mediterranean water in the Atlantic Iberian margin reveals early isolation events during the Messinian Salinity Crisis. Glob. Planet. Chang. 231, 104297.
Butiseacă, G.A., Van der Meer, M.T., Kontakiotis, G., Agiadi, K., Thivaiou, D., Besiou, E., Vasiliev, I., 2022. Multiple crises preceded the Mediterranean Salinity Crisis: Aridification and vegetation changes revealed by biomarkers and stable isotopes. Glob. Planet. Chang. 217, 103951.
Castradori, D., 1998. Calcareous nannofossils in the basal Zanclean of the Eastern Mediterranean Sea: remarks on paleoceanography and sapropel formation. In: Proceedings-Ocean Drilling Program Scientific Results, pp. 113–124.
Corbí, H., Soria, J.M., Giannetti, A., Yébenes, A., 2020. The step-by-step restriction of the Mediterranean (start, amplification, and consolidation phases) preceding the Messinian Salinity Crisis (climax phase) in the Bajo Segura basin. Geo-Mar. Lett. 40, 341–361.
Corselli, C., Principato, M.S., Maffioli, P., Crudeli, D., 2002. Changes in planktonic assemblages during sapropel S5 deposition: evidence from Urania Basin area, eastern Mediterranean. Paleoceanography 17 (3), 1–30.
De La Rocha, C.L., Passow, U., 2007. Factors influencing the sinking of POC and the efficiency of the biological carbon pump. Deep-Sea Res. II Top. Stud. Oceanogr. 54 (5–7), 639–658.
De Lange, G.J., Thomson, J., Reitz, A., Slomp, C.P., Speranza Principato, M., Erba, E., Corselli, C., 2008. Synchronous basin-wide formation and redox-controlled preservation of a Mediterranean sapropel. Nat. Geosci. 1 (9), 606–610.
Di Stefano, A., Verducci, M., Lirer, F., Ferraro, L., Iaccarino, S.M., Hüsing, S.K., Hilgen, F. J., 2010. Paleoenvironmental conditions preceding the Messinian Salinity Crisis in the Central Mediterranean: integrated data from the Upper Miocene Trave section (Italy). Palaeogeogr. Palaeoclimatol. Palaeoecol. 297 (1), 37–53.
Diaz, R.J., Rosenberg, R., 2008. Spreading dead zones and consequences for marine ecosystems. Science 321 (5891), 926–929.
Duarte, C.M., Regaudie-de-Gioux, A., Arrieta, J.M., Delgado-Huertas, A., Agustí, S., 2013. The oligotrophic ocean is heterotrophic. Annu. Rev. Mar. Sci. 5, 551–569.
Flecker, R., Krijgsman, W., Capella, W., de Castro Martíns, C., Dmitrieva, E., Mayser, J.P., Yousfi, M.Z., 2015. Evolution of the Late Miocene Mediterranean–Atlantic gateways and their impact on regional and global environmental change. Earth Sci. Rev. 150, 365–392.
Flores, J.A., Sierro, F.J., Filippelli, G.M., Bárcena, M.Á., Pérez-Folgado, M., Vázquez, A., Utrilla, R., 2005. Surface water dynamics and phytoplankton communities during deposition of cyclic late Messinian sapropel sequences in the western Mediterranean. Mar. Micropaleontol. 56 (1–2), 50–79.
Foster, G.L., Hull, P., Lunt, D.J., Zachos, J.C., 2018. Placing our current 'hyperthermal' in the context of rapid climate change in our geological past. Philos. Trans. R. Soc. A Math. Phys. Eng. Sci. 376 (2130), 20170086.

Gennari, R., Lozar, F., Turco, E., Dela Pierre, F., Lugli, S., Manzi, V., Taviani, M., 2018. Integrated stratigraphy and paleoceanographic evolution of the pre-evaporitic phase of the Messinian salinity crisis in the Eastern Mediterranean as recorded in the Tokhni section (Cyprus island). Newsl. Stratigr. 51 (1), 33–55.

Gennari, R., Lozar, F., Natalicchio, M., Zanella, E., Carnevale, G., Dela Pierre, F., 2020. Chronology of the Messinian events in the northernmost part of the Mediterranean: the Govone section (Piedmont Basin, NW Italy). Riv. Ital. Paleontol. Stratigr. 126 (2), 541–560.

Gennari, R., Lugli, S., Manzi, V., Persico, D., Reghizzi, M., Roveri, M., 2024. Stress precursors of the Messinian salinity crisis as recorded by calcareous plankton and geochemistry in the Eastern Mediterranean: the Upper Metochia section of the Gavdos Island (Greece). Palaeogeogr. Palaeoclimatol. Palaeoecol. 636, 111970.

Ghielmi, M., Minervini, M., Nini, C., Rogledi, S., Rossi, M., Vignolo, A., 2010. Sedimentary and tectonic evolution in the eastern Po-Plain and northern Adriatic Sea area from Messinian to Middle Pleistocene (Italy). Rendiconti Lincei 21, 131–166.

Gibbs, S.J., Shackleton, N.J., Young, J.R., 2004. Identification of dissolution patterns in nannofossil assemblages: a high-resolution comparison of synchronous records from Ceara rise, ODP Leg 154. Paleoceanography 19 (1).

Giorgi, F., 2006. Climate change hot-spots. Geophys. Res. Lett. 33 (8).

Giraudeau, J., 1992. Distribution of recent nannofossils beneath the Benguela system: southwest African continental margin. Mar. Geol. 108 (2), 219–237.

Gladstone, R., Flecker, R., Valdes, P., Lunt, D., Markwick, P., 2007. The Mediterranean hydrologic budget from a late Miocene global climate simulation. Palaeogeogr. Palaeoclimatol. Palaeoecol. 251 (2), 254–267.

Glock, N., Roy, A.S., Romero, D., Wein, T., Weissenbach, J., Revsbech, N.P., Dagan, T., 2019. Metabolic preference of nitrate over oxygen as an electron acceptor in foraminifera from the Peruvian oxygen minimum zone. Proc. Natl. Acad. Sci. 116 (8), 2860–2865.

Grothe, A., Andreetto, F., Reichart, G.J., Wolthers, M., Van Baak, C.G., Vasiliev, I., Krijgsman, W., 2020. Paratethys pacing of the Messinian Salinity Crisis: Low salinity waters contributing to gypsum precipitation? Earth Planet. Sci. Lett. 532, 116029.

Hammer, Ø., Harper, D.A., 2001. Past: paleontological statistics software package for educaton and data anlysis. Palaeontol. Electron. 4 (1), 1.

Hemleben, C., Spindler, M., Anderson, O.R., Hemleben, C., Spindler, M., Anderson, O.R., 1989. Taxonomy and species features. Modern Planktonic Foraminifera 8–32.

Hilgen, F.J., 1991. Astronomical calibration of Gauss to Matuyama sapropels in the Mediterranean and implication for the geomagnetic polarity time scale. Earth Planet. Sci. Lett. 104 (2–4), 226–244.

Hüsing, S.K., Kuiper, K.F., Link, W., Hilgen, F.J., Krijgsman, W., 2009. The upper Tortonian–lower Messinian at Monte Dei Corvi (Northern Apennines, Italy): completing a Mediterranean reference section for the Tortonian stage. Earth Planet. Sci. Lett. 282 (1–4), 140–157.

Iaccarino, S.M., Bertini, A., Di Stefano, A., Ferraro, L., Gennari, R., Grossi, F., Angeletti, L., 2008. The Trave section (Monte Dei Corvi, Ancona, Central Italy): an integrated paleontological study of the Messinian deposits. Stratigraphy 5 (3–4), 281–306.

Jannink, N.T., Zachariasse, W.J., Van der Zwaan, G.J., 1998. Living (Rose Bengal stained) benthic foraminifera from the Pakistan continental margin (northern Arabian Sea). Deep-Sea Res. I Oceanogr. Res. Pap. 45 (9), 1483–1513.

Kallel, N., Paterne, M., Duplessy, J.C., Vergnaudgrazzini, C., Pujol, C., Labeyrie, L., Pierre, C., 1997. Enhanced rainfall in the Mediterranean region during the last sapropel event. Oceanol. Acta 20 (5), 697–712.

Kidd, R.B., Cita, M.B., Ryan, W.B.F., 1978. Stratigraphy of eastern Mediterranean sapropel sequences recovered during DSDP leg 42A and their paleoenvironmental significance. Initial Rep. Deep Sea Drill Proj. 42, 421–443.

Kontakiotis, G., Butiseacă, G.A., Antonarakou, A., Agiadi, K., Zarkogiannis, S.D., Krsnik, E., Vasiliev, I., 2022. Hypersalinity accompanies tectonic restriction in the eastern Mediterranean prior to the Messinian Salinity Crisis. Palaeogeogr. Palaeoclimatol. Palaeoecol. 592, 110903.

Kouwenhoven, T.V., Van der Zwaan, G.J., 2006. A reconstruction of late Miocene Mediterranean circulation patterns using benthic foraminifera. Palaeogeogr. Palaeoclimatol. Palaeoecol. 238 (1–4), 373–385.

Kouwenhoven, T.J., Seidenkrantz, M.S., Van der Zwaan, G.J., 1999. Deep-water changes: the near-synchronous disappearance of a group of benthic foraminifera from the late Miocene Mediterranean. Palaeogeogr. Palaeoclimatol. Palaeoecol. 152 (3–4), 259–281.

Kouwenhoven, T.J., Morigi, C., Negri, A., Giunta, S., Krijgsman, W., Rouchy, J.M., 2006. Paleoenvironmental evolution of the eastern Mediterranean during the Messinian: Constraints from integrated microfossil data of the Pissouri Basin (Cyprus). Mar. Micropaleontol. 60 (1), 17–44.

Kranner, M., Harzhauser, M., Beer, C., Auer, G., Piller, W.E., 2022. Calculating dissolved marine oxygen values based on an enhanced Benthic Foraminifera Oxygen Index. Sci. Rep. 12 (1), 1376.

Krijgsman, W., Gaboardi, S., Hilgen, F.J., Iaccarino, S., Kaenel, E.D., Laan, E.V.D., 2004. Revised astrochronology for the Ain el Beida section (Atlantic Morocco): no glacio-eustatic control for the onset of the Messinian Salinity Crisis. Stratigraphy 1, 87–101.

Krijgsman, W., Capella, W., Simon, D., Hilgen, F.J., Kouwenhoven, T.J., Meijer, P.T., Flecker, R., 2018. The Gibraltar corridor: Watergate of the Messinian salinity crisis. Mar. Geol. 403, 238–246.

Krijgsman, W., Palcu, D.V., Andreetto, F., Stoica, M., Mandic, O., 2020. Changing seas in the late Miocene Northern Aegean: a Paratethyan approach to Mediterranean basin evolution. Earth Sci. Rev. 210, 103386.

Krom, M.D., Herut, B., Mantoura, R.F.C., 2004. Nutrient budget for the Eastern Mediterranean: Implications for phosphorus limitation. Limnol. Oceanogr. 49 (5), 1582–1592.

Kwon, E.Y., Primeau, F., Sarmiento, J.L., 2009. The impact of remineralization depth on the air–sea carbon balance. Nat. Geosci. 2 (9), 630–635.

Laskar, J., Robutel, P., Joutel, F., Gastineau, M., Correia, A.C., Levrard, B., 2004. A long-term numerical solution for the insolation quantities of the Earth. Astron. Astrophys. 428 (1), 261–285.

Lazzari, P., Mattia, G., Solidoro, C., Salon, S., Crise, A., Zavatarelli, M., Vichi, M., 2014. The impacts of climate change and environmental management policies on the trophic regimes in the Mediterranean Sea: scenario analyses. J. Mar. Syst. 135, 137–149.

Limburg, K.E., Breitburg, D., Swaney, D.P., Jacinto, G., 2020. Ocean deoxygenation: a primer. One Earth 2 (1), 24–29.

Lionello, P., Scarascia, L., 2018. The relation between climate change in the Mediterranean region and global warming. Reg. Environ. Chang. 18, 1481–1493.

Lozar, F., Violanti, D., Pierre, F.D., Bernardi, E., Cavagna, S., Clari, P., Trenkwalder, S., 2010. Calcareous nannofossils and foraminifera herald the Messinian salinity crisis: the Pollenzo section (Alba, Cuneo; NW Italy). Geobios 43 (1), 21–32.

Lozar, F., Violanti, D., Bernardi, E., Dela Pierre, F., Natalicchio, M., 2018. Identifying the onset of the Messinian salinity crisis: a reassessment of the biochronostratigraphic tools (Piedmont Basin, NW Italy). Newsl. Stratigr. 51 (1), 11–31.

Macias, D.M., Garcia-Gorriz, E., Stips, A., 2015. Productivity changes in the Mediterranean Sea for the twenty-first century in response to changes in the regional atmospheric forcing. Front. Mar. Sci. 2, 79.

Mancini, A.M., Gennari, R., Ziveri, P., Mortyn, P.G., Stolwijk, D.J., Lozar, F., 2020. Calcareous nannofossil and foraminiferal trace element records in the Sorbas Basin: a new piece of the Messinian Salinity Crisis onset puzzle. Palaeogeogr. Palaeoclimatol. Palaeoecol. 554, 109796.

Mancini, A.M., Grelaud, M., Ziveri, P., Nallino, E., Lozar, F., 2021. Calcareous nannofossil size and abundance response to the Messinian Salinity Crisis onset and paleoenvironmental dynamics. Paleoceanograph. Paleoclimatol. 36 (9) e2020PA004155.

Mancini, A.M., Gennari, R., Natalicchio, M., Pierre, F.D., Carnevale, G., Pastero, L., Lozar, F., 2022. Taphonomic bias on calcareous micro and nannofossils and paleoenvironmental evolution across the Messinian Salinity Crisis onset: Insights from the Sorbas Basin (SE Spain). Palaeogeogr. Palaeoclimatol. Palaeoecol. 599, 111056.

Mancini, A.M., Gennari, R., Lozar, F., Natalicchio, M., Della Porta, G., Bernasconi, D., Negri, A., 2024a. Sensitivity of the thermohaline circulation during the Messinian: toward constraining the dynamics of Mediterranean deoxygenation. Deep-Sea Res. I Oceanogr. Res. Pap. 203, 104217.

Mancini, A.M., Lozar, F., Gennari, R., Capozzi, R., Morigi, C., Negri, A., 2024b. The past to unravel the future: Deoxygenation events in the geological archive and the anthropocene oxygen crisis. Earth Sci. Rev. 104664.

Mayser, J.P., Flecker, R., Marzocchi, A., Kouwenhoven, T.J., Lunt, D.J., Pancost, R.D., 2017. Precession driven changes in terrestrial organic matter input to the Eastern Mediterranean leading up to the Messinian Salinity Crisis. Earth Planet. Sci. Lett. 462, 199–211.

MedECC, 2020. Summary for Policymakers. In: Cramer, W., Guiot, J., Marini, K. (Eds.), Climate and Environmental Change in the Mediterranean Basin – Current Situation and Risks for the Future. First Mediterranean Assessment Report. Union for the Mediterranean, Plan Bleu, UNEP/ MAP, Marseille, France, pp. 11–40.

Meijer, P.T., 2006. A box model of the blocked-outflow scenario for the Messinian Salinity Crisis. Earth Planet. Sci. Lett. 248 (1–2), 486–494.

Montanari, A., Beaudoin, B., Chan, L.S., Coccioni, R., Deino, A., DePaolo, D.J., Stankiewicz, A., 1995. Chapter E1 Integrated stratigraphy of the Middle to Upper Miocene pelagic sequence of the Conero riviera (Marche region, Italy). In: Developments in Palaeontology and Stratigraphy, vol. 15. Elsevier, pp. 409–450.

Murray, J.W., 2006. Ecology and Applications of Benthic Foraminifera. Cambridge University Press.

Nittis, K., Lascaratos, A., 1998. Diagnostic and prognostic numerical studies of LIW formation. J. Mar. Syst. 18 (1–3), 179–195.

Pellegrino, L., Abe, K., Gennari, R., Lozar, F., Pierre, F.D., Natalicchio, M., Carnevale, G., 2020. Integrated micropaleontological study of the Messinian diatomaceous deposits of the Monferrato Arc (Piedmont basin, NW Italy): New insights into the paleoceanographic evolution of the northernmost Mediterranean region. Mar. Micropaleontol. 160, 101910.

Perch-Nielsen, K., 1985. Cenozoic calcareous nannofossils. Plankton Stratigraph. 427–455.

Popov, S.V., Rozanov, A.Y., Rögl, F., Steininger, F.F., Shcherba, I.G., Kovac, M., 2004. Lithological-paleogeographic maps of Paratethys. CFS Cour. Forschungsinstitut Senckenberg 250, 1–46.

Powley, H.R., Krom, M.D., Van Cappellen, P., 2017. Understanding the unique biogeochemistry of the Mediterranean Sea: Insights from a coupled phosphorus and nitrogen model. Glob. Biogeochem. Cycles 31 (6), 1010–1031.

Reale, M., Cossarini, G., Lazzari, P., Lovato, T., Bolzon, G., Masina, S., Salon, S., 2022. Acidification, deoxygenation, and nutrient and biomass declines in a warming Mediterranean Sea. Biogeosciences 19 (17), 4035–4065.

Renaud, S., Ziveri, P., Broerse, A.T., 2002. Geographical and seasonal differences in morphology and dynamics of the coccolithophore Calcidiscus leptoporus. Mar. Micropaleontol. 46 (3–4), 363–385.

Richon, C., Dutay, J.C., Bopp, L., Le Vu, B., Orr, J.C., Somot, S., Dulac, F., 2019. Biogeochemical response of the Mediterranean Sea to the transient SRES-A2 climate change scenario. Biogeosciences 16 (1), 135–165.

Riforgiato, F., Foresi, L.M., Aldinucci, M., Mazzei, R., Donia, F., Gennari, R., Sandrelli, F., 2008. Foraminiferal record and astronomical cycles: an example from the Messinian pre-evaporitic Gello Composite Section (Tuscany, Italy). Stratigraphy 5 (3–4), 265–280.

Rohling, E.J., Marino, G., Grant, K.M., 2015. Mediterranean climate and oceanography, and the periodic development of anoxic events (sapropels). Earth Sci. Rev. 143, 62–97.
Roveri, M., Boscolo Gallo, A., Rossi, M., Gennari, R., Iaccarino, S.M., Lugli, S., Taviani, M., 2005. The Adriatic foreland record of Messinian events (central Adriatic Sea, Italy). GeoActa 4 (139), 158.
Roveri, M., Flecker, R., Krijgsman, W., Lofi, J., Lugli, S., Manzi, V., Stoica, M., 2014. The Messinian Salinity Crisis: past and future of a great challenge for marine sciences. Mar. Geol. 352, 25–58.
Sabino, M., Schefuß, E., Natalicchio, M., Pierre, F.D., Birgel, D., Bortels, D., Peckmann, J., 2020. Climatic and hydrologic variability in the northern Mediterranean across the onset of the Messinian salinity crisis. Palaeogeogr. Palaeoclimatol. Palaeoecol. 545, 109632.
Sakalli, A., 2017. Sea surface temperature change in the Mediterranean Sea under climate change: a linear model for simulation of the sea surface temperature up to 2100. Appl. Ecol. Environ. Res. 15, 707–716.
Sanchez-Gomez, E., Somot, S., Mariotti, A., 2009. Future changes in the Mediterranean water budget projected by an ensemble of regional climate models. Geophys. Res. Lett. 36 (21).
Schiebel, R., Hemleben, C., 2017. Planktic Foraminifers in the Modern Ocean.
Schiebel, R., Waniek, J., Bork, M., Hemleben, C., 2001. Planktic foraminiferal production stimulated by chlorophyll redistribution and entrainment of nutrients. Deep-Sea Res. I Oceanogr. Res. Pap. 48 (3), 721–740.
Schroeder, K., Garcìa-Lafuente, J., Josey, S.A., Artale, V., Nardelli, B.B., Carrillo, A., Zodiatis, G., 2012. Circulation of the Mediterranean Sea and its variability. Climat. Mediterranean Region 187.
Schroeder, K., Tanhua, T., Chiggiato, J., Velaoras, D., Josey, S.A., Lafuente, J.G., Vargas-Yáñez, M., 2023. The forcings of the Mediterranean Sea and the physical properties of its water masses. In: Oceanography of the Mediterranean Sea. Elsevier, pp. 93–123.
Sierro, F.J., Flores, J.A., Zamarreno, I., Vázquez, A., Utrilla, R., Francés, G., Krijgsman, W., 1999. Messinian pre-evaporite sapropels and precession-induced oscillations in western Mediterranean climate. Mar. Geol. 153 (1–4), 137–146.
Sierro, F.J., Hilgen, F.J., Krijgsman, W., Flores, J.A., 2001. The Abad composite (SE Spain): a Messinian reference section for the Mediterranean and the APTS. Palaeogeogr. Palaeoclimatol. Palaeoecol. 168 (1–2), 141–169.
Sierro, F.J., Flores, J.A., Francés, G., Vazquez, A., Utrilla, R., Zamarreño, I., Barcena, M. A., 2003. Orbitally-controlled oscillations in planktic communities and cyclic changes in western Mediterranean hydrography during the Messinian. Palaeogeogr. Palaeoclimatol. Palaeoecol. 190, 289–316.
Simon, D., Marzocchi, A., Flecker, R., Lunt, D.J., Hilgen, F.J., Meijer, P.T., 2017. Quantifying the Mediterranean freshwater budget throughout the late Miocene: New implications for sapropel formation and the Messinian Salinity Crisis. Earth Planet. Sci. Lett. 472, 25–37.
Somot, S., Sevault, F., Déqué, M., 2006. Transient climate change scenario simulation of the Mediterranean Sea for the twenty-first century using a high-resolution ocean circulation model. Clim. Dyn. 27, 851–879.
Stachowitsch, M., Riedel, B., Zuschin, M., 2012. The return of shallow shelf seas as extreme environments: Anoxia and Macrofauna Reactions in the Northern Adriatic Sea. In: Altenbach, A.V. (Ed.), Anoxia: Evidence for Eukaryote Survival and Paleontological Strategies. Springer, pp. 353–368.
Taylforth, J.E., McCay, G.A., Ellam, R., Raffi, I., Kroon, D., Robertson, A.H., 2014. Middle Miocene (Langhian) sapropel formation in the easternmost Mediterranean deep-water basin: evidence from northern Cyprus. Mar. Pet. Geol. 57, 521–536.
Turley, C.M., 1999. The changing Mediterranean Sea—a sensitive ecosystem? Prog. Oceanogr. 44 (1–3), 387–400.
Tzanova, A., Herbert, T.D., Peterson, L., 2015. Cooling Mediterranean Sea surface temperatures during the late Miocene provide a climate context for evolutionary transitions in Africa and Eurasia. Earth Planet. Sci. Lett. 419, 71–80.
Tzevahirtzian, A., Caruso, A., Andreetto, F., Bonomo, S., Krijgsman, W., 2023. A bio-chronostratigraphic study of the upper Miocene from the northern Caltanissetta Basin, Sicily (core 3AGN2S04). Implications for dating the Messinian Salinity Crisis onset. Sediment. Geol. 445, 106330.
UNEP, 1996. Assessment of the state of eutrophication in the Mediterranean Sea. In: MAP Technical Report Series, 106, p. 211.
Van der Zwaan, G.J., Jorissen, F.J., De Stigter, H.C., 1990. The depth dependency of planktonic/benthic foraminiferal ratios: constraints and applications. Mar. Geol. 95 (1), 1–16.
Vasiliev, I., Karakitsios, V., Bouloubassi, I., Agiadi, K., Kontakiotis, G., Antonarakou, A., Pasadakis, N., 2019. Large sea surface temperature, salinity, and productivity-preservation changes preceding the onset of the Messinian Salinity Crisis in the eastern Mediterranean Sea. Paleoceanograph. Paleoclimatol. 34 (2), 182–202.
Viaroli, P., Nizzoli, D., Pinardi, M., Soana, E., Bartoli, M., 2015. Eutrophication of the Mediterranean Sea: a watershed—cascading aquatic filter approach. Rendiconti Lincei 26, 13–23.
Violanti, D., Lozar, F., Natalicchio, M., Dela Pierre, F., Bernardi, E., Clari, P., Cavagna, S., 2013. Stress-tolerant microfossils of a Messinian succession from the Northern Mediterranean basin (Pollenzo section, Piedmont, northwestern Italy). Boll. Soc. Paleontol. Ital. 52 (1), 46.
Volkmann, R., 2000. Planktic foraminifer ecology and stable isotope geochemistry in the Arctic Ocean: implications from water column and sediment surface studies for quantitative reconstructions of oceanic parameters. Reports on Polar Research. PhD Thesis, AWI Bremerhaven.
Wade, B.S., Bown, P.R., 2006. Calcareous nannofossils in extreme environments: the Messinian salinity crisis, Polemi Basin, Cyprus. Palaeogeogr. Palaeoclimatol. Palaeoecol. 233 (3–4), 271–286.
Winter, A., 1994. Biogeography of living coccolithophores in ocean waters. Coccolithophores 161–177.
Ziveri, P., Baumann, K.H., Böckel, B., Bollmann, J., Young, J.R., 2004. Biogeography of Selected Holocene Coccoliths in the Atlantic Ocean. From Molecular Processes to Global Impact, Coccolithophores, pp. 403–428.